AALTO UNIVERSITY
School of Science and Technology
Faculty of Electronics, Communication and Automation
Department of Signal Processing and Acoustics

Juha Holm

Applying the Finite Element Method for Modelling Loudspeaker Waveguide Directivity

Master's Thesis submitted in partial fulfillment of the requirements for the degree of Master of Science in Technology.

Iisalmi, May 6, 2010

Supervisor:	Prof. Vesa Välimäki
Instructor:	Dr. Aki Mäkivirta, D.Sc

Author:	Juha Holm
Name of the thesis:	Applying the Finite Element Method for Modelling Loudspeaker Waveguide Directivity
Date:	May 6, 2010
Number of pages:	59 + vii
Faculty:	Electronics, Communication and Automation
Professorship:	S-89
Supervisor:	Prof. Vesa Välimäki
Instructors:	Dr. Aki Mäkivirta, D.Sc

Directivity has a great influence on a loudspeaker's perceived performance. Indoors directivity defines the indirect sound heard which influences the timbre and spatial perception. Outdoors the directivity defines the sound heard off-axis of the speaker where most of the audience is.

The directivity of a single transducer primarily depends on driver size. Directivity can be modified using an acoustical waveguide. The primary purpose of a waveguide is to control the directivity of the source, but increased efficiency is a favourable side-effect.

This thesis concentrates on applying the Finite Element Method (FEM) to virtually prototype waveguides. The theory of FEM and its usability in acoustics is reviewed. Also theory for horn directivity is discussed. Major emphasis is on reviewing and developing a method for visualizing modelled and measured directivity in a comparable manner.

There are three major outputs of the thesis. First, the method of virtual prototyping is validated by comparing and analyzing the measured and FEM modelled prototypes. Also the value of the method as a designing tool is emphasized. Second, a visualization tool is created to enable comparison and analysis of the modelled and measured directivity. Third, a new method is created for combining a FEM model and laser velocimetry of a driver. The presented approach increases the accuracy of the model because the driver excitation can be made more realistic.

Keywords: Loudspeaker, Directivity, Waveguide, Horn, Acoustics, Finite Element Method, FEM, Modelling

Tekijä:	Juha Holm
Työn nimi:	Elementtimenetelmän soveltaminen kaiuttimen akustisen aaltosuuntaimen suuntaavuuden mallintamiseen
Päivämäärä:	6.5.2010
Sivuja:	59 + vii
Tiedekunta:	Elektroniikka, tietoliikenne ja automaatio
Professuuri:	S-89
Työn valvoja:	Prof. Vesa Välimäki
Työn ohjaaja:	TkT Aki Mäkivirta

Kaiuttimen suuntaavuus on yksi merkittävä tekijä kaiuttimen suorituskykyä arvioitaessa. Sisätiloissa suuntaavuus määrittää ihmisen kuuleman epäsuoran äänen. Epäsuora ääni vaikuttaa havaittuun äänen väriin sekä tilan tuntuun. Ulkotilojen äänentoistossa vain harva kuulija on kaiuttimen suoralla linjalla. Tällöin kaiuttimen suuntaavuus määrää kuullun äänen värin, koska ulkotiloissa heijastuksia on vähän. Yksittäisen kaiutinelementin suuntaavuus on riippuvainen lähinnä sen koosta. Yksi tapa äänilähteen suuntaavuuden muokkaamiseen on akustisen suuntaimen käyttäminen. Suuntain parantaa myös äänilähteen hyötysuhdetta.

Diplomityö keskittyy esittelemään elementtimenetelmän soveltamista akustisen suuntaimen suunnittelussa. Elementtimentelmä on tietokonepohjainen numeerinen mallinnusmenetelmä, jota voidaan käyttää akustisten kenttien mallintamiseen. Työssä esitellään suuntaimen suuntaavuuden teoriaa ja kuinka suuntaavuus vaikuttaa ihmisen havaitsemaan ääneen. Työssä esitellään menetelmiä suuntaavuuden graafiseen esittämiseen vertailtavalla ja ymmärrettävällä tavalla.

Työllä on kolme päätulosta. Ensinnäkin todennetaan elementtimallinnuksen käyttökelpoisuus suuntaimen suunnittelussa. Mallinnettuja ja mitattuja prototyypin suuntaavuuksia verrataan ja eroavaisuuksia analysoidaan. Toinen työn tulos on kehitetty työkalu mallinnetun ja mitatun suuntaavuuden graafiseen esittämiseen havainnollisella tavalla. Kolmas tulos liittyy mallinnuksen ja mittauksen yhdistämiseen. Mallinnuksen lopputuloksen tarkkuutta voitiin parantaa yhdistämällä malliin kaiutinelementin mitattu nopeus taajuuden funktiona.

Avainsanat: kaiutin, suuntaavuus, aaltosuuntain, torvi, elementtimenetelmä, FEM, akustiikka, mallintaminen

Acknowledgements

I want to thank my instructor Dr. Aki Mäkivirta for the numerous and creative discussions we had. It has been unique position for me to get to know a person who has such a combination of experience and jovial passion for learning. I also want to thank my supervisor Prof. Vesa Välimäki for the constructive feedback given during the work.

I thank Jussi Väisänen for sharing his experience of designing loudspeakers as a system. I thank Ilkka Rissanen for the creative feedback about the measurement setup. I admire Juha Urhonen's MATLAB skills and I am grateful to him for sharing his knowledge. I thank Stephen Millar for always questioning the results and sharing his knowledge of CAD skills. I thank Darren Rose for motivating discussions and his work on improving the language of the thesis.

Lastly I want to thank Genelec Oy for providing the intellectual environment for the project. I had the privilege to dedicate my work to the subject which the thesis is based. Special thanks for creating this opportunity goes to Dr. Siamäk Naghian, the Director of Research & Development.

Iisalmi, May 6, 2010

Juha Holm

Contents

Symbols and abbreviations

BEM	Boundary Element Method
DOF	Degrees of Freedom
DUT	Device Under Test
EMF	Electromagnetic Force
FFT	Fast Fourier Transform
FEM	Finite Element Method
MLS	Maximum Length Sequence
PA	Public Address
PDE	Partial Differential Equation
SPL	Sound Pressure Level

1 Introduction

Producing sound is a simple, but sometimes a complex matter. The first musical instruments date back thousands of years ago. The era of reproduced music began in the late nineteenth century with the introduction of the gramophone and its predecessors. The era of amplified music began in the 1920s, when Kellogg & Rice patented the moving coil loudspeaker. Virtually all current loudspeakers are based on the same principle introduced back then. Billions of audio devices are built every year. Therefore it is fair to say that they are really ubiquitous. Nevertheless, even the most advanced sound systems cannot match the fidelity of live sound at its best. The main driving force behind the thesis is to understand and create tools to improve the listening experience. As the story ahead will tell, sometimes it is necessary to go quite far from the original idea of listening experience to be able to find ways to improve it.

This thesis combines FEM (Finite Element Method) modelling and acoustical understanding of directivity and waveguides. The goal is to use modelling to virtually prototype loudspeakers. The motivation is to speed up the prototyping process and reduce the amount of costly prototypes. The author also has a stubborn belief that modelling can lead to better performing loudspeakers in the end. This can be explained by the low threshold of trying out new ideas by virtual prototyping and also the enhanced understanding given by the advanced visualization methods.

In general, waveguide and horn are synonyms. The primary purpose of early horn designs was to increase the output of the sound system. Later it became obvious that horns have a beneficial effect on the loudspeaker directivity. For some applications, the directivity characteristics of the horn are the main benefit and increased sensitivity is a side-effect [1]. These horns designed for directivity are called waveguides to emphasize the different design goals compared to horns. These days the devices used for public address sound reinforcement are called horns. Respectively the devices used in home speakers and studio monitors are called waveguides.

Figure 1.1. A loudspeaker with a waveguide – Genelec 8040A.

A common goal of a waveguide is to match the directivity of a high frequency transducer to the directivity of a low frequency transducer (Figure 1.1). The waveguide is located on the upper part of the speaker, around the high frequency transducer, called a tweeter. The purpose of the waveguide is to control the dispersion characteristics of the sound source. Above the crossover frequency the directivity of the high frequency driver should be controlled. In general, the goal is to achieve constant beam width of the acoustical radiation or slightly decreasing beam width towards high frequencies.

1.1 The aim of the work

The content of the thesis is based on the work done on modelling acoustical waveguides while working for Genelec Oy. In this thesis are discussed the problems and solutions encountered when developing a method for modelling waveguide directivity.

Analytical solutions are available for only a waveguide geometries and those are not feasible designs for the targeted directivity characteristics. Nevertheless there are some rules of thumb available for waveguide design. These rules are discussed and also evaluated during the test case of the thesis.

By definition, the accuracy of a model is always second to the real world. The selected method for validating the accuracy of the model is to compare it against the real world. There is no ready made tool for visualizing measurements and modelled results in comparable form. Therefore a major emphasis is needed on developing and creating tools for visualizing directivity.

One aim of the work is to verify the accuracy of the method. Therefore reasoning is needed to evaluate the sources of the error of the model. Inaccuracy in the modelling result does not necessarily make the tool useless. However it is essential to understand the limits of the tool.

A test case is created for comparing the measured and modelled results. The shape of the waveguide is chosen to be far from the optimal design. The reasoning for the selection is that there would be more acoustical phenomena present. Modelling should be able to expose these undesired effects. After all, the motivation for the use of modelling is to reveal and minimize these unwanted effects.

1.2 Outline

The outline of the thesis is divided into twelve chapters. The first chapter contains the introduction, aim and outline of the thesis. The second chapter discusses the acoustic wave equation, which is the basis of modelling acoustic fields. The third chapter discusses the use of FEM for solving the wave equation, splitting complex geometry to small elements and previous work done in the field of transducer and waveguide modelling. The fourth chapter concentrates on the sound source and room interaction, its subjective importance and how it is related to the directivity of the source. Also other aspects of sound quality are reviewed in order to widen the perspective. The fifth chapter introduces the directivity visualization methods used now and in the past. The sixth chapter discusses the directivity of a circular piston source. This reveals the directivity characteristics typical for the most commonly used sound sources. The seventh chapter expands the directivity discussion to horns. The directivity of several well known horn profiles is discussed.

The eighth chapter covers the methods used in the FEM modelling. The ninth chapter discusses measurement methods for the physical prototype and visualization methods to enable the comparison of the measured and modelled waveguide.

The tenth chapter analyzes the phenomena found in the FEM modelled waveguide. The emphasis is on introducing the modelling as an engineering tool.

In the eleventh chapter the results of the model and measurement are shown and analyzed. The comparison is done for the directivity of the waveguide and also for the frequency response of the waveguide. The twelfth chapter contains the conclusion of the work. The purpose of the chapter is to summarize the results and discuss future of the FEM modelling.

2 Time-harmonic solution of the wave equation

The basis of solving acoustic fields is the three-dimensional wave equation (Equation (2.1). The wave equation is the basis when deriving the physics necessary for solving FEM. The medium is assumed to be lossless. The wave equation is based on the conservation of mass. Therefore no fluid flow should be present when it is used [2]. On the right hand side of the wave equation there is a possible monopole source $\mathbf{Q}$. On the left hand side there is the second time derivative of the pressure p and a constant term which consists of the density of air ρ_0 and the speed of sound in air c. In the middle there is difference of gradient of pressure ∇p and possible dipole source $\mathbf{q}$. The difference is divided by density of air ρ_0 and divergence operation $\nabla \cdot$ is taken.

$$\frac{1}{\rho_0 c^2}\frac{\delta^2 p}{\delta t^2} + \nabla \cdot \left(-\frac{1}{\rho_0}(\nabla p - \mathbf{q}) \right) = \mathbf{Q} \tag{2.1}$$

The wave equation can be significantly simplified if the pressure is time-harmonic. In other words, the modelling is done in the frequency domain and transient phenomena are left out.

For a time-harmonic wave, the pressure in three-dimensional space must be time harmonic (Equation (2.2). The variable $\mathbf{x}$ is a three-dimensional vector coordinate, variable t is time and ω is angular velocity.

$$p(\mathbf{x},t) = p(\mathbf{x})e^{i\omega t} \tag{2.2}$$

If the source and the problem are time-harmonic, the wave-equation can be written in time-harmonic form (Equation (2.3) [3].

$$\nabla \cdot \left(-\frac{1}{p_0}(\nabla p - \mathbf{q}) \right) - \frac{\omega^{'2} p}{\rho_0 c} = \mathbf{Q} \tag{2.3}$$

Where $p = p(\mathbf{x}, \omega)$, hence it is a three-dimensional and frequency domain solution.

The frequency domain solution of the wave equation presented above is also known as the Helmholtz equation.

Reducing the analysis to 2D axisymmetric geometry significantly reduces the computational cost of solving the model. The computational cost for various

geometries is discussed in the Chapter 3.3. Fortunately many acoustic problems are 2D axisymmetrical, for example loudspeaker driver cone and waveguide. 3D geometry is axisymmetric if it can be represented by a 2D profile and defined axis of rotation which extrudes it to a 3D geometry.

For a time-harmonic wave, the pressure in the 2D axisymmetric space (Equation (2.4) is dependent on the radial coordinate r, the axial coordinate z, the azimuthal angle φ and the circumferential wave number m [3].

$$p(r,z,\varphi) = p(r,z)e^{-im\varphi} \tag{2.4}$$

It is noteworthy that azimuthal angle φ affects only to the phase of the pressure. This is the key for reduced computational cost of the 2D axisymmetric geometries. Equation (2.3 and Equation (2.4 can be merged to Helmholtz equation of 2-dimensional axisymmetric space (Equation (2.5) [3].

$$\frac{\delta}{\delta r}\left[-\frac{r}{\rho_0}\left(\frac{\delta p}{\delta r}-q_r\right)\right]+r\frac{\delta}{\delta z}\left[-\frac{1}{\rho_0}\left(\frac{\delta p}{\delta z}-q_z\right)\right]-\left[\left(\frac{\omega}{c}\right)^2-\left(\frac{m}{r}\right)^2\right]\frac{rp}{\rho_0}=r\mathbf{Q} \quad (2.5$$

3 Using the FEM to solve the wave equation

The use of the FEM for engineering problems originated in the mechanical engineering and the aeronautical industry as early the late 1950s [4]. FEM was first used for applications where failure of the end product would be costly and even fatal. Examples of such applications are bridges and aircraft.

An analytical solution of an acoustic field is only available to a few simple geometries. For more complex geometries, a method called the FEM can be used. The basic idea of the method is to divide a geometrically complex system into smaller individual components, which are called elements. The solution for these small and geometrically simple elements is straightforward to obtain.

Error in the FEM model is caused by three reasons. First is the inaccuracy in the geometry. Second is the inaccuracy of the physics. Third is the finite element size, which causes computational error.

Usually the inaccuracies of geometry and physics dominate the overall error. Considering the computational cost, it is not reasonable to push the error caused by finite element size much below the overall error [5].

	Highest frequency to be modelled	Sampling rate	Time domain calculations	Frequency resolution
Time domain solution	20 kHz	40 kHz	256 samples	156 Hz
	Highest frequency to be modelled	-	Frequency domain calculations (1 kHz to 20 kHz)	Frequency resolution
Frequency domain solution	20 kHz	-	95	200 Hz

Table 3.1. Computational cost of the time-domain modelling versus frequency domain modelling.

With the acoustic simulation, usually the frequency response is the most interesting result. One approach to obtain the frequency response would be the same as with most modern acoustic measurement systems: somehow achieve the impulse response of the system and calculate frequency response with a fast fourier transform (FFT) of

the impulse response. Similarly it is also possible to model the impulse response of the system and obtain frequency response. However the computational cost of this approach is very high. The computational cost of calculating time-domain solutions for the FEM is much higher than calculating frequency domain solutions. For a time domain solution 256 calculations are needed in time domain compared to the 95 calculations of the frequency domain solution (Table 3.1). Therefore it is more feasible to directly calculate the amplitudes at the frequencies of interest.

3.1 Discretization the geometry to elements

The fundamental idea of the FEM is to divide the geometrically complicated partial differential equation problem down to a coupled group of smaller problems. Each small problem is called an element. The process of dividing the geometry is called meshing. There are several locations to specify the physics on each mesh element. The basic approach is to specify the wave equation state parameters to the corners of the element (Figure 3.1). It is also possible to specify the states to the edges of the element or even to the centre of the element. These state parameters are called degrees of freedom (DOF). Using higher order elements improves the accuracy of the simulation, because there are more state parameters calculated per element. Of course the computational cost is also increased. In the models in this thesis a second order Lagrange element is used. Therefore there is a degree of freedom in each corner of the element and also at the sides of the elements.

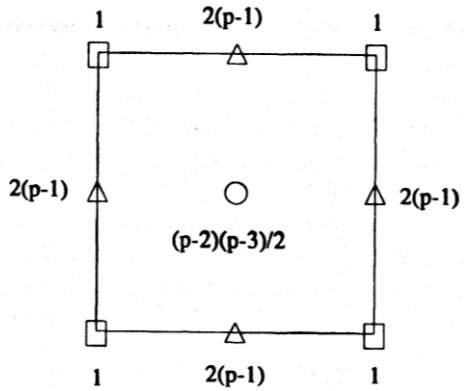

Figure 3.1. Degrees of freedom of each mesh element. Adopted from [3].

3.2 Selection of the element size

The distribution of the geometry to elements is called meshing. The maximum size of the element is limited by two factors. The first limiting factor is the shortest wavelength to be calculated. The second limitation is the size of the geometry details to be modelled.

Usually these constraints are related to each other. Small details become interesting only when they are comparable to the wavelength of interest. Of course this depends on the phenomenon. For example, Helmholtz resonance might a have significant influence on the modelled result, even if the port opening is small related to the wavelength.

$$EL_{\max} = \frac{c}{6 f_{\max}} \tag{3.1}$$

Maximum element size should be smaller than one-sixth of the wavelength of the acoustical wave (Equation (3.1) [5]. According to the Nyquist theorem, the element size should be smaller than half of the wavelength so that solution would have any meaning [3].

3.3 The concept of degrees of freedom

The number of degrees of freedom determines the computational cost of solving the model. It is dependent on the mesh element count of the model. This is contradictory to the need for a detailed model and large air space to approximate far field conditions. The number of degrees of freedom is also highly dependent on whether the problem is 1D, 2D or 3D (Table 3.2). An approximation of the degrees of freedom of the model can be calculated, if constant y, domain size A, wavelength λ and exponential x are known (Equation (3.2).

Geometry	Multiplying constant y	Modelled domain size A	Wavelength λ exponential x
1D or 1D axisymmetric	12	Length	1
2D or 2D axisymmetric	144	Area	Squared
3D	1828	Volume	Cubed

Table 3.2. Factors affecting the degrees of freedom with 1D, 2D and 3D geometries [5].

$$DOF = y \cdot A \cdot \lambda^x \tag{3.2}$$

According to the table and equation presented, the degrees of freedom can be significantly reduced if a 3D geometry can be reduced to a 2D geometry. It is possible to solve an axisymmetric 3D problem in a 2D domain without extra computational cost. This feature is very fortunate in the field of acoustics. Often geometries related to acoustics are axisymmetric or at least a reasonable axisymmetric approximation can be made. This is true also in the case of waveguide design.

3.4 Computational cost example

An approximation of the degrees of freedom for 1D, 2D and 3D problems were introduced in the previous chapter. However it is not straightforward to understand the difference in computational cost between a 2D axisymmetric and a full 3D model. Therefore the following example is shown to justify the use axisymmetry whenever possible.

Geometry	Edge length of the model geometry [m]	Modelled domain size	Wavelength at 20 kHz [mm]	Wavelength exponential	Degrees of freedom
2D-axisymmetric	0.4	$0.16\ m^2$	3.4	2	78 000
3D	0.4	$0.064\,m^3$	3.4	3	23 000 000

Table 3.3. Example calculation of degrees of freedom with 2D-axisymmetric and 3D model.

Assume an axisymmetric system that can be modelled either as a full 3D model or a 2D axisymmetric model. The length of the model edges is 0.4 meters and the highest frequency of interest is 20 kHz. Degrees of freedom of the 2D-axisymmetric and full 3D geometry can be approximated with the known theory (Equation (3.2 and Table 3.2). The number of the DOF for 2D axisymmetric model is 78000 (Table 3.3). Solving 78 thousand degrees of freedom takes about 10 seconds per frequency with a modern desktop computer. The memory requirement is less than 1 GB.

For a full 3D model the degrees of freedom is 23 million. The problem is too large to be solved with a desktop computer because of the memory requirement. According

to this example it can be concluded that 3D modelling is limited either to small frequencies or small geometries (or supercomputers).

The limit of the degrees of freedom to be calculated with a desktop computer is from one to two million. However, with long calculation times the FEM modelling is rather a verification tool than an interactive design tool.

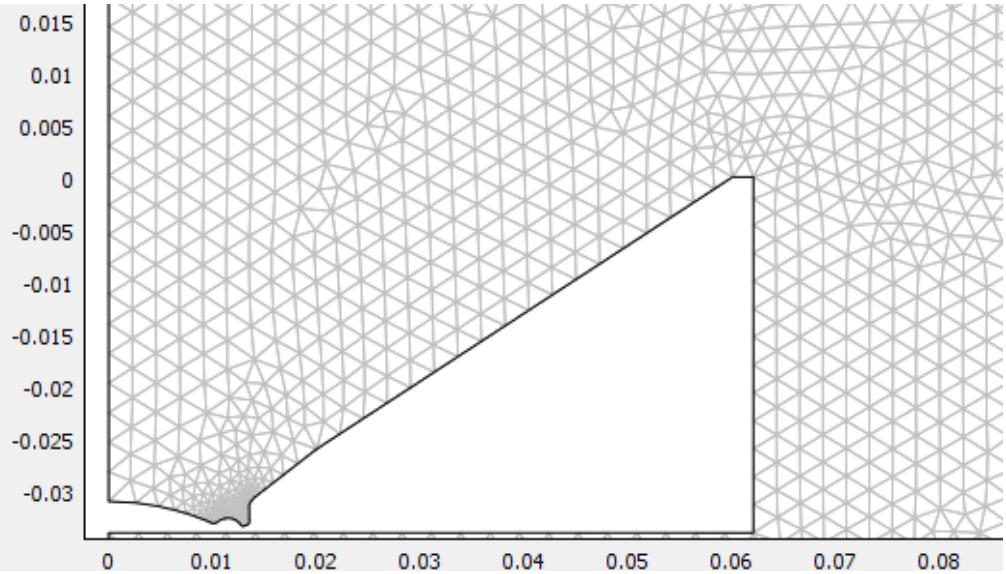

Figure 3.2. Mesh around the waveguide.

In this thesis prototype the highest frequency of interest is 20 kHz. According to the one sixth of the wavelength rule (Equation (3.1) the maximum element size is 0.5 mm. Figure 3.2 shows the mesh around the waveguide. This mesh is used in all the calculations of the FEM based models. It easy to see that the element size is quite constant over the domain. However, around the tweeter surround and faceplate the mesh is denser. This is caused by the small details in geometry around that area. The small details have an influence on the directivity at high frequencies. Therefore the extra computational cost caused by the small details is justified.

3.5 Applications of the finite element method to acoustics

The use of FEM for acoustical modelling is not a new idea. This chapter discusses the most important papers and applications. Emphasis is on the topics of waveguide and transducer modelling.

In the 1980s a Japanese research group published papers of applying FEM for solving loudspeaker related acoustical problems. In 1982, Kyouno used vibro-acoustic coupling for compression driver and horn [6]. He explained the theoretical background of coupling the mechanical and acoustical domain with FEM. An elastical diaphragm of a compression driver was modelled in the mechanical domain with two-way coupling to the acoustical domain of a horn. Both cone vibrations and the near field acoustic field in the horn was investigated. Far field sound pressure was approximated with an analytical equation. Enlightening conclusions were made based on the model and measurements. First, the diaphragm vibration has little effect on the directivity characteristics of a system with a compression driver. Second, the acoustic load coupling to the diaphragm has great effect on its vibration. Thirdly, the assumption of plane wave or spherical wave shape of radiation is not valid at high frequencies - therefore the analytical solutions are not valid either.

In 2001, Martin Opitz described three important tools for optimizing miniature loudspeakers for mobile applications [7]. FEM was used to optimize the force factor Bl and linearity and suspension compliance linearity. The structure of the magnet circuit was optimized with FEM. Mobile transducers should be flat as possible, but the efficiency of the magnet system sacrifices if the iron parts saturate because of small material thickness. Therefore these two contradictory requirements should be optimized. Also the membrane material thickness and geometry is optimized with a mechanical FEM model as is the linearity of the suspension. Mechanical vibrations were coupled to the acoustical world by using BEM (Boundary Element Method). Results were compared to physical prototype measured with laser velocitymetry.

Mark Dodd has done extensive research on research on modelling loudspeakers with FEM. In 2002, Dodd modelled loudspeaker motor thermal behaviour with the FEM. He modelled the heat spreading from voice coil with axisymmetric geometry of the complete driver. Both static and transient cases were studied. He explained the four heat paths: radiation, conduction, natural convection and forced convection. Convection is the most difficult phenomenon to model, because the physics model changes from low velocity laminar flow to high velocity turbulent flow. Dodd found agreement between modelled and measured results. In 2003 Dodd published his first paper with electro-magneto-mechanical-acoustical interaction [8]. Because full two-way interaction between domains would have been too complicated to calculate, the

problem was divided into parts and parameterized one-way results were used for coupling. The design case was developing a phase-plug for compression driver. Blocked coil impedance was calculated with transient magnetic FEM, force factor with magneto-static FEM. Input voltage and voice coil length could be defined. These parameters were enough to define the force affecting the fully coupled vibro-acoustic FEM model and thus obtain the full model of the driver. Compression drivers are always combined with a horn, which defines the acoustical impedance seen by the compression driver throat. This variable was eliminated by modelling and measuring the drivers in an impedance tube, which provides a purely resistive termination to the horn mouth. Then phase-plug cavity geometry was optimized with the model described above. The accuracy of the final design was also compared with measurements. A simplified compression driver model was coupled with a horn. There was basic agreement with the model and measurements, but the causes for differences were not analyzed. In 2006, Dodd expanded the FEM based optimization to diaphragm and waveguide geometry [9]. He analyzed the theoretical solution of A planar piston in an infinite baffle. Unfortunately he did not compare the result with the well known analytical solution. Also the radiation of a hemispherical diaphragm was studied. With analysis of a finite length conical waveguide, he pointed out the problem caused by the mouth reflection. The last example was about a realistic dome and waveguide shape. The contours in the directivity sonogram behaved very well. He also presented a directivity sonogram of the impulse response of the system. This approach gave insight to the shape of wavefronts in a waveguide.

In 2007, Biba et al used FEM for developing the moving parts of a headphone transducer [10]. The mechanical vibrations of the transducer membrane were modelled with FEM and vibro-acoustic interaction with the BEM. Visco-thermal effects were modelled in the narrow regions of the model. Cushion and similar damping elements were modelled with frequency dependent transfer impedances. The model was done in real 3D because the surround had corrugations and therefore axisymmetric modelling could not be used. The publication was divided to three phases. First, the moving parts of the transducer were modelled with FEM. Modelling results were compared to the average acceleration derived from measurements in a vacuum. As usual, there was agreement with results although the high frequency modelling is not very exact. Second, the air load was included in the

model. The influence of the slit elements and magnet circuit behind the transducer was investigated. Also a phase plug was added in front of the transducer. Third, the cushioning surround of the transducer was added. Adding details to the model also adds sources of error. However, the basic phenomena were visible both in measured and modelled curves. After all, this paper was a rare insight to headphone transducer design.

In 2007, Backman presented a paper where he compared analytical solutions of various acoustical phenomena to more realistic FEM models [11]. He studied the impedances of transmission lines. The main point was to excite the transmission line with a non-planar wave. The conclusion was that one-dimensional solutions successfully predict the few lowest nodes of the impedance tube. Second, he modelled the acoustical length of the port with several flare radii. The conclusion was, that the lumped parameter model is accurate for predicting the fundamental resonance frequency of a box with port, but not accurate enough to predict the open pipe resonances of the port if a back wall or flared edges are present. One detail to criticize is that Backman used acoustic simulation software, which does not take in account the turbulent airflow inside the port [2].

4 The subjective importance of the directivity

The purpose of this chapter is to motivate the importance of the source directivity to the sound perceived by the listener. First is a literature review on the factors affecting to the human preference of the sound and what is the contribution of the directivity Second is discussed the loudspeaker and room interaction.

4.1 Human preference for sound

Comparison of loudspeakers' performance has been under discussion as long as they have been built. It would be desirable that, the subjective performance of a speaker could be evaluated with objective measurements. Toole has done extensive work on evaluating loudspeaker subjective performance [12][13][14]. His findings were unambiguous. In general, flat on-axis frequency response is preferred over inconsistent response [13]. Likewise a low level of nonlinear distortion is preferred over high a level of distortion [14]. Toole also paid great attention to the loudspeaker and room interaction, which is dependent on the loudspeaker directivity. These finding are discussed in detail in the following paragraphs.

According to Toole, a controlled change of frequency response towards an off-axis direction is preferred over abrupt changes [13]. This concept is called controlled directivity. The concept is very loosely specified. Defining the directivity is further discussed in Chapter 5.

The sound heard in a room is dependent on the room, the speaker and the signal transmitted to the speaker. In this work the emphasis is on the speaker performance and how it can be evaluated. However room acoustics is briefly covered to highlight the importance of the loudspeaker directivity characteristics. The effect of the loudspeaker signal source is out of the scope of the thesis.

4.2 Loudspeaker and room interaction

The following is an analysis of the factors affecting the measured impulse response of a speaker in a room. The assumptions are that the speaker is in a room, its acoustical axis is towards the listening position and there are not obstacles in the line of sight between the speaker and the listening position (Figure 4.1). The impulse response specifies change between the input signal of the system and the pressure at the listening position. The only missing variable is the listener. Therefore impulse response should closely correlate to the sound perceived by the listener.

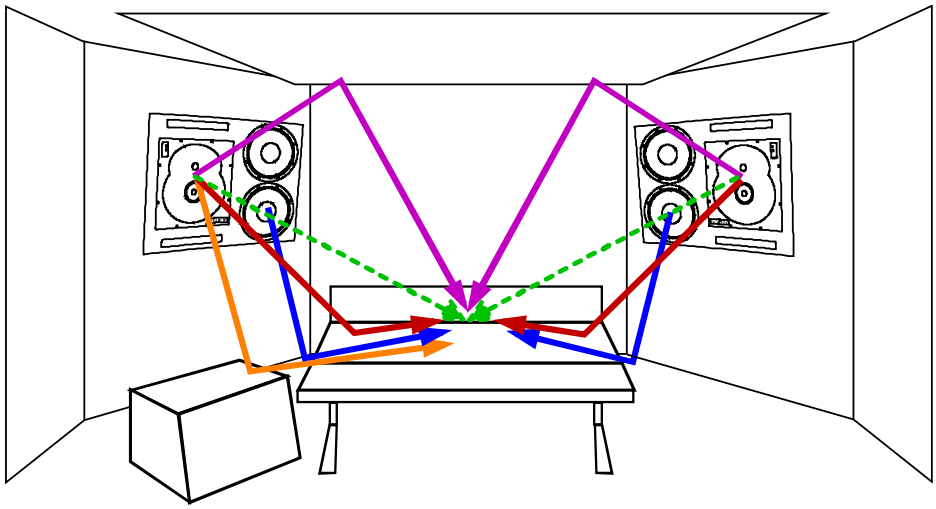

Figure 4.1. Direct sound (green), boundary reflections (magenta, red, orange) at a listening position of a music studio.

One approach to analyze the loudspeaker and room interaction is to look at the energy decay at the listening position (Figure 4.2). The energy decay curve is a logarithmic presentation of a squared impulse response. As the figure shows, the sound heard at the listening position can be divided to three parts.

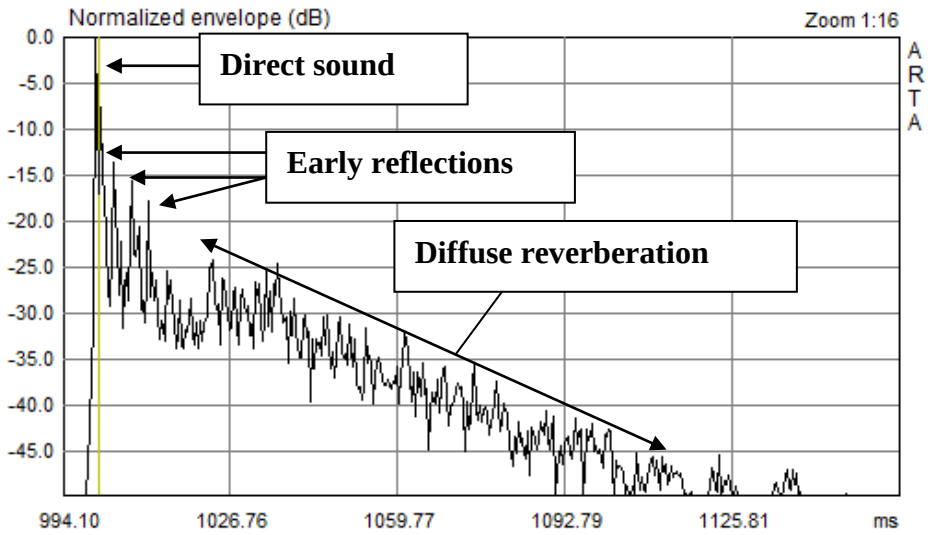

Figure 4.2. The energy decay curve of a loudspeaker in a room. Measured at the listening position of a music studio.

First, the direct sound arrives. With a reasonable listening arrangement, there are no obstacles in the line of sight between the listening position and the speaker (Figure 4.1). Likewise the speaker acoustical axis is turned towards the listening position, which is now on referred to on-axis response. Therefore the direct sound depends only on the loudspeaker on-axis frequency response. The direct sound is marked in Figure 4.2, which usually is the highest peak of the impulse response.

Second, the early reflections arrive (Figure 4.2). These are usually first order reflections from the side walls, floor and ceiling (Figure 4.1). The time difference between the direct sound and early reflections is dependent on the wave travel time difference. Early reflections contribute to the spatial and tonal perception of the sound. The spatial effect is more easily understood by considering the time domain signal presented. The time delay and amplitude of the reflection gives a clue to the auditory system about the spatial space. Early reflections also affect the tonal balance. The sound absorption of the reflecting surfaces is frequency dependent. With a steady state signal, the direct and delayed reflected sound interferes at the listening position, which causes a comb filtering effect in the frequency domain.

Third, the diffuse reverberation is left (Figure 4.2). Reverberation consists of a countless number of reflections from the room boundaries e.g. it is diffuse. The diffuse reverberation contributes to the perceived spatial experience. It takes a certain time for diffuse reverberation to build up. Therefore there is a silent part in the impulse response between the early reflections and constantly attenuating diffuse

reverberation. Diffuse reverberation also affects the tonal balance of the sound, because absorption coefficients of the room material are frequency dependent. It is common that the reverberation time is longer at the low frequencies.

When analyzing the three phenomena seen in the impulse response, it is noteworthy that only the direct sound is defined by the on-axis frequency response. Despite of the fact, the on-axis response is one of the most used measures to evaluate loudspeaker performance. Early reflections are dependent on the room acoustics and off-axis response of the speaker at the relevant angle. Diffuse reverberation is dependent on room acoustics and total power emitted by the speaker i.e. power response.

To conclude, it is generally agreed that subjective loudspeaker performance is largely specified by following characteristics: on-axis frequency response, directivity and distortion [1] [14]. This thesis concentrates on the directivity.

5 Representing directivity

This chapter presents the known ways to visualize directivity. In the simplest form the directivity is presented as a single scalar number that is a function of frequency (Directivity factor (Q), Directivity index (DI) and Beam width). It is noteworthy that the mathematics behind these presentation methods is most complicated, because of the need to compress a four-dimensional information to one scalar number.

The second step is to show the frequency response at the specific points of the space (Frequency response) or one polar arc of the directivity at a specific frequency (Polar diagram). The problem with these plots is that many lines are needed present comprehensive information about the directivity.

The third group are the 3D graphs. Either a full 3D pressure response balloon of the radiated sound at a specific frequency can be presented (Balloon graph) or equal amplitude contours of one polar plane as function of frequency (Directivity plot). The limitation of the balloon graph is that only one frequency can be shown at a time. The limitation of the directivity plot is that only one plane can be shown at once.

5.1 Source radiation in space

Consider a sound source in a space that is located at the origin of the axes (Figure 5.1). Around the source are the polar arcs of the horizontal plane and vertical plane. The sound source is radiating to space and thus its radiation is a three-dimensional problem. Its radiation is also a function of frequency and therefore a full expression of a directivity is four-dimensional problem. Unfortunately four-dimensional problems cannot be visualized in an understandable form. Therefore there have been several methods compressing the directivity information to one constant, one-dimensional, two-dimensional or three-dimensional graph. But it is noteworthy that no graph can express the source directivity completely. The fewer dimensions, the more compromises have to be made.

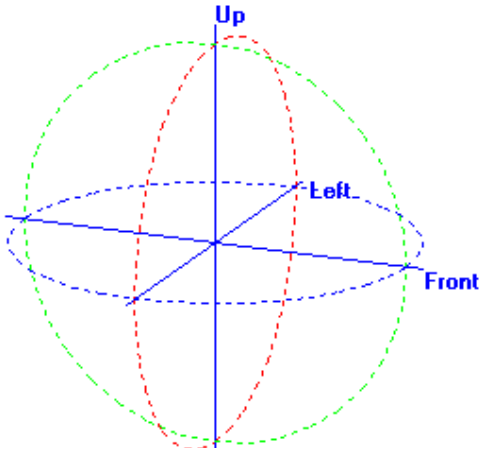

Figure 5.1. Loudspeaker and the planes. Loudspeaker in the origin, vertical plane (blue), horizontal plane (green).

The target of expressing directivity with numbers or a graph has been to compress the four-dimensional information to form that would be informative and describe the directivity characteristics enough and at the same time being understandable and easy to compare with other sources

5.2 Directivity factor (Q)

Directivity factor can be seen as a ratio between on-axis pressure and the total sound power radiated by the speaker. In exact form, it is ratio between the sound power P_{AN} and P_{AD}. Its definition is given as [15]:

$$Q = \frac{P_{AN}}{P_{AD}} \tag{5.1}$$

Where P_{AN} is defined in Equation (5.2. It is a sound power that would be radiated by an omnidirectional (i.e. point source) source with on-axis pressure p at distance r [15].

$$P_{AN} = \frac{4\pi r^2 p^2}{\rho c} \tag{5.2}$$

P_{AD} is the total sound power emitted by the source (Equation (5.3). Angles θ and φ used in the equation are the azimuth and vertical angle to the on-axis direction (Figure 5.2).

$$P_{AD} = \frac{r^2}{\rho c} \int_0^{2\pi} \int_0^{\pi} p^2(\theta, \varphi, r) \sin(\theta) d\theta d\varphi \tag{5.3}$$

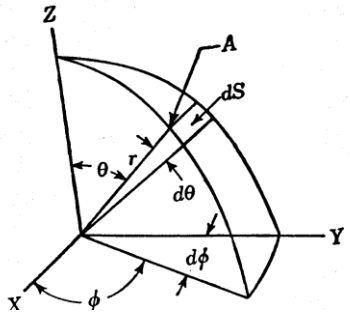

Figure 5.2. Coordinate system. Adopted from [16].

Some very useful room acoustic parameters can be calculated when Directivity factor Q is known. The sound pressure level L_p at distance r from source can be calculated (Equation (5.4) when the directivity factor Q of the source, sound power level of the source L_w, radiation space Ω in sterians and amount of absorption A is known [17].

$$L_p = L_w + 10 \log \left[\frac{Q}{\Omega r^2} + \frac{4}{A} \right] \tag{5.4}$$

The reverberation radius r_R (Equation (5.5) is the radius where the sound power of the direct sound and reverberant sound from the source are equal. It can be solved from Equation (5.4 [17]:

$$r_R = \sqrt{\frac{QA}{4\Omega}} \tag{5.5}$$

5.3 Directivity index (DI)

Directivity index (Equation (5.6) is the directivity factor Q in a logarithmic form. It is more commonly used than the directivity factor. It is defined as [15].

$$DI = \log_{10} Q \tag{5.6}$$

The DI index is widely used in the loudspeaker industry. Its benefit is that it is rather easy to calculate from the commonly measured on-axis frequency response and horizontal and vertical polar measurements. It can be presented as a single curve that is a function of frequency.

The drawback is that DI simplifies the off-axis radiation. The root of this problem is that sound power is integrated over all angles. Therefore sources with very different radiation characteristic may still have equal on-axis pressure response and power response, and therefore have equal directivity indeces.

5.4 Beam width

Beam width presents the width of the main lobe of the sound source. The main lobe is defined as an angle of -6 dB attenuation compared to the on-axis response that is a function of frequency. This information is already available in polar plots. Therefore the beam width can be seen as post-processing of polar plots to show the directivity information in a single graph. The benefit is good frequency resolution. The downside is that only the -6 dB curve is available, which does not comprehensively describe directivity characteristic of the source.

The beam width graph usability is at best at public address systems for outdoor events. Then the beam width provides indication of how large area can be relatively uniformly covered with a single source.

5.5 Polar diagram

The polar diagram shows the amplitude of the source on a horizontal or a vertical plane (Figure 5.1). The polar plot depicts amplitude of a source at a certain frequency as a function of angle (Figure 5.3). Usually the polar response is normalized to the on-axis response. Therefore on-axis response has 0 dB and amplitudes at the polar angles are relative and usually lower than the on-axis amplitude.

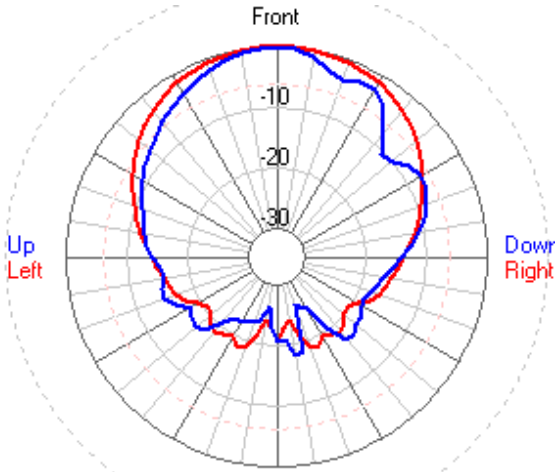

Figure 5.3. Polar diagram of a 2-way speaker at 3 kHz. Horizontal (red) and vertical (blue) planes.

The advantage of the polar plot is the accurate angle resolution. Single graphs are also easy to compare. The disadvantage is that only few frequencies can be shown in one graph with good readability. Therefore several graphs are needed to see a large enough frequency range, which compromises the readability of the result.

5.6 Frequency response

A simple way to visualize directivity is to plot several frequency responses at different locations on the polar planes (Figure 5.4). The advantage of this visualization is a good frequency resolution. The source has to be measured only at the angles of interest. Therefore the measurement is fast and can be made without a turntable. The disadvantage is the limited angle resolution, because only a few responses can be shown with good readability.

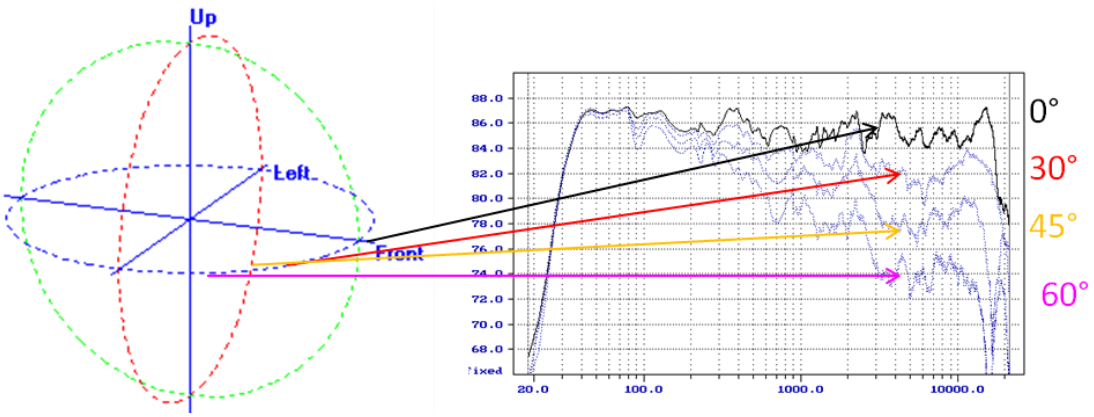

Figure 5.4. Frequency responses of horizontal plane.

5.7 Balloon graph

Imagine that the every point on the surface of the balloon (Figure 5.5) has its own frequency response. If only one frequency is viewed at the time, a graph may be made where the colour and position of the points describe the amplitude in that direction. This can be also seen as a 3D equivalent for traditional polar plots introduced before. The advantage of this visualization is that full 3D radiation can be shown at once. The disadvantage is that only one frequency can be presented per graph.

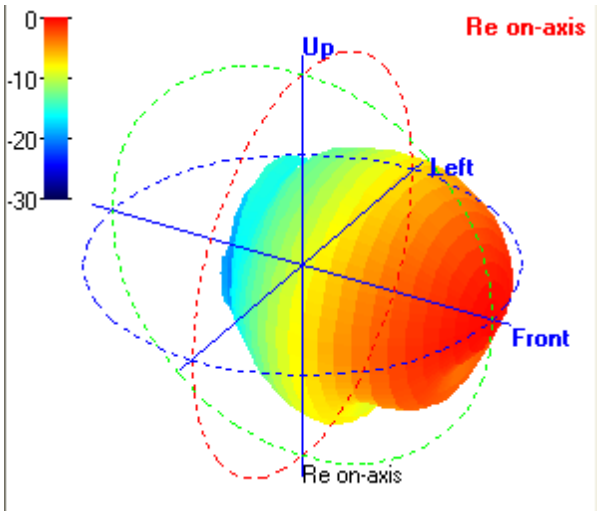

Figure 5.5. Balloon graph of two-way speaker at 3 kHz

5.8 Directivity plot

The directivity contour plot can be seen as an extension of the beam width curve. Information about the beam width is enhanced by adding the contours of other dB limits. Usually the resolution is from 0 dB to -21 dB in 3 dB increments. The readability of the plot has been improved by adding colours between the amplitude contours. Adding the colours can also been seen as converting the graph to a three dimensional representation. In a way, the directivity contour diagram combines the advantages of polar plots and beam width curves. The downside is the trade off between the frequency resolution and the readability of the graph. The amplitude resolution of the contours has to be large enough to maintain the readability.

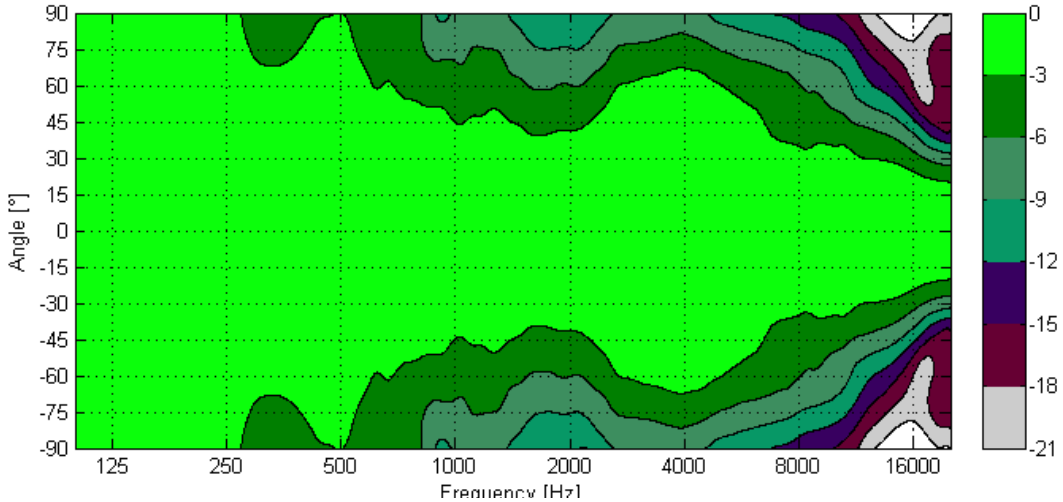

Figure 5.6. Directivity of direct radiating two-way speaker.

An example of a directivity plot (Figure 5.6) is from two-way speaker horizontal plane measurements. The plot is for a horizontal angle from -90° to 90°, to achieve clear view of the front half of the radiation of the speaker. The directivity change at the crossover frequency is clearly visible. The measured loudspeaker does not have a waveguide.

6 The directivity of a direct radiator

The directivity of the circular piston source is relevant for several reasons, although the topic of the thesis is waveguide directivity. It is common combine direct radiating sources and sources with a waveguide in a loudspeaker. Usually the goal of the design is to match the directivity of these sources. Therefore it is essential to understand the elements affecting direct radiating source directivity. Also, in some cases the directivity of a waveguide can be described as the directivity of a plane circular piston.

The directivity of a loudspeaker is highly frequency dependent. The analytical solution for directivity of circular piston source in an infinite baffle does exist (Equation (6.2) [15]). The circular piston source radiation directivity is dependent on the variable called wave number ka (Equation (6.1), which is related to the circumference of the piston $2\pi r$ and the wavelength λ.

$$ka = \frac{2\pi r}{\lambda} \tag{6.1}$$

With the wave number known, the directivity at an angle α can be calculated with a first order Bessel function J_1 (Equation (6.2).

$$R_a = \frac{2J_1(ka\sin\alpha)}{ka\sin\alpha} \tag{6.2}$$

One way to express the directivity of a circular piston source is to show the polar plots at certain ka-numbers (Figure 6.1). The following three features can be found when analyzing the directivity of a circular piston source. First, a circular piston source is omnidirectional when the wave number ka < 1. Second, when ka >1, the beam width narrows towards high frequencies and the source is no longer omnidirectional. Third, with higher ka < 4, side lobes are present in addition to the main lobe. At this wave number the wavelength is shorter than the diameter of the source. Thus sound radiated from different parts of the piston is in and out of phase which causes constructive and destructive interference in off-axis directions.

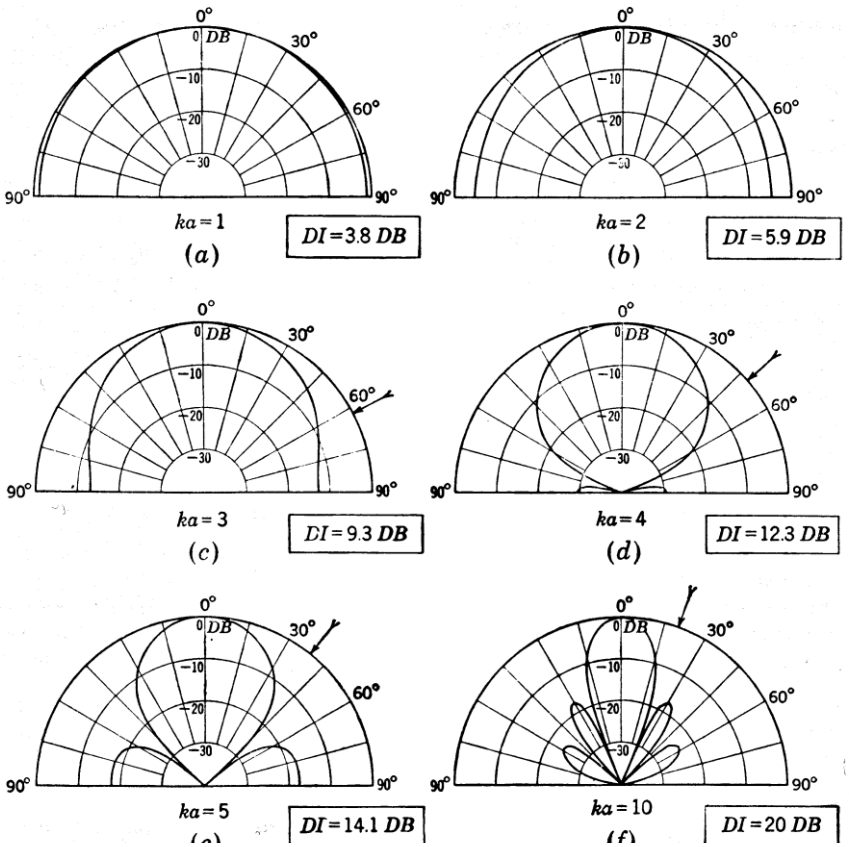

Figure 6.1. Directivity of a circular piston source. Adopted from [16].

Direct radiator directivity performance has a major influence on loudspeaker design. These acoustical phenomena limit the usability of direct radiating sources for loudspeakers.

Based on the analysis of the circular piston directivity, three conclusions can be made considering a loudspeaker design. First, the beam width of a large cone might be too narrow at high frequencies to cover the desired area or then the side lobes limit the usability. Second, the beam width of the piston might be too broad for the application, thus causing high SPL levels at an undesired location. This is problem arises especially with low frequency sources. Third, ratio between direct sound and power response of the direct radiator is a function of frequency. Therefore the ratio between direct and reflected sound is not constant as a function of frequency.

7 The directivity of a horn radiator

The directivity of a horn has been of interest as long horn loaded sources have been made. Therefore it is surprising how little information about the directivity of horns can be found in the literature. Again, the probable reason for this is the lack analytical solutions. Therefore horn directivity has been more of an engineering problem solved with prototypes and intuition. The academic world has shown relatively little interesting for this topic. Most papers published concentrate on the final shape achieved for a commercial application. Very little is discussed about the reasoning that led to the solution, probably because of trade secrets.

Despite the efforts made for finding sources for horn directivity, the success of finding solid text was thin. The most comprehensive source found for this thesis was Olson's work on the subject published back in 1957 [15]. The theory presented in this chapter is largely based on Olson's research.

When discussing the directivity of a horn, it is essential to keep in mind the directivity characteristics of a direct radiator presented in Chapter 6. It is common to combine direct radiator and horn loaded radiator in loudspeaker systems.

The theory part of the horn directivity chapter is divided into two parts. First the directivity of an exponential horn is discussed. Exponential horn has been historically of great interest because of two reasons. First, there is an analytical solution for designing an exponential horn. Second, exponential horn has good impedance match between source mechanical impedance and the impedance of air.

The second topic of discussion is the directivity of a conical horn. The conical horn has been used a lot because it is the most straightforward geometry of the horn imaginable. It also shows an interesting phenomenon toward high frequencies.

7.1 The exponential horn

The cross-sectional area S of an exponential horn follows an Equation (7.1. The constants are the throat area S_1 and the flaring constant m of the horn and variable distance x from the throat [15].

$$S = S_1 e^{mx} \tag{7.1}$$

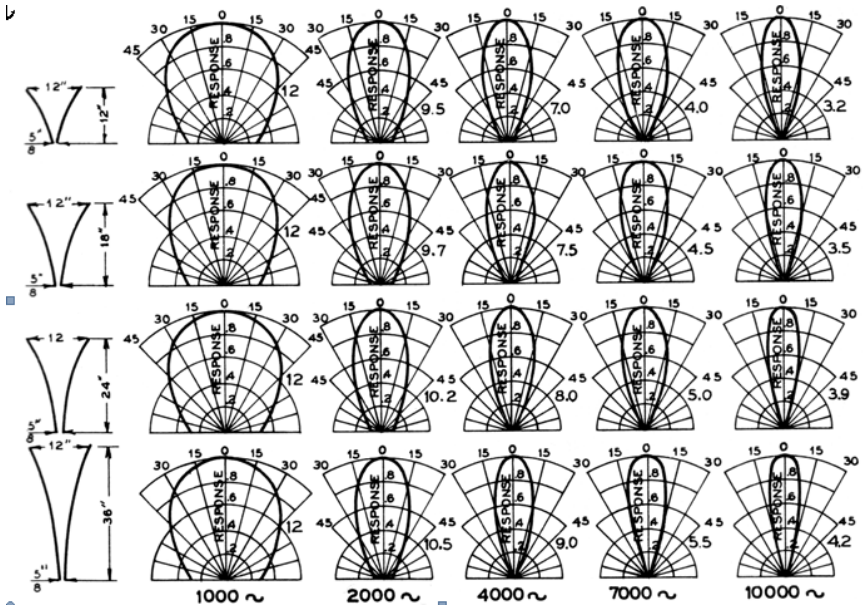

Figure 7.1. Exponential horn with constant mouth size and varying length. Adopted from [15].

One approach to research the directivity properties of a horn is to compare polar plots of several horn geometries (Figure 7.1). The throat and mouth circumferences are constant, but the length and flare rate are varying. The beam width decreases towards high frequencies, which is a universal feature for exponential horn. The following problems arise because of this feature. First, the narrow beam at high frequencies limits the area that can be covered with a single horn unit. Second, the power response of the source decreases towards high frequencies, which affects the room response of the speaker.

The number at the right side of each polar diagram indicates the size of a circular piston, which would have equal directivity to this particular horn. At 1000 Hz, the length of the exponential horn does not affect the directivity of the horn. The directivity of the horn is equal to the directivity of a circular piston with diameter of 12 inches, which is exactly the diameter of the horn mouth. For frequencies from 2

kHz to 10 kHz the horn length does matter. With a longer horn, the beam width is slightly decreased at mid and high frequency range.

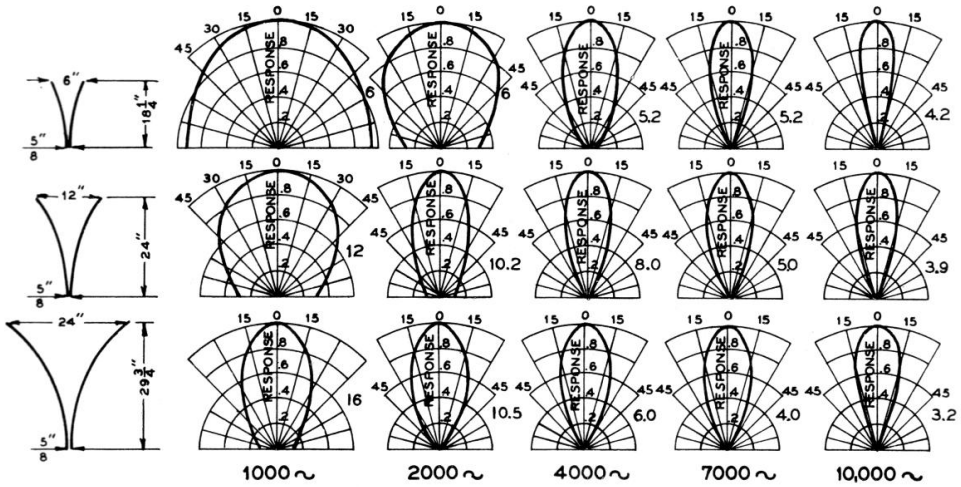

Figure 7.2. Exponential horn with varying mouth size. Adopted from [15].

Another approach is to keep the flare rate m constant (Figure 7.2). Mouth size and length are varying. Again mouth the size is defining the directivity at low frequencies. With 6 inch and 12 inch mouth diameter horns the directivity at 1 kHz is comparable to the directivity of a direct radiator with an equal diameter. With a long horn and a large mouth, the directivity is more constant as a function of frequency. This is because the horn length and mouth are large compared to the wavelength and therefore the directivity is defined by the horn geometry rather than size of the mouth.

7.2 The conical horn

The conical horn has different directivity characteristics (Figure 7.3). In the figure is presented polar plots of two conical horns with varying length, but constant mouth and throat size. The effect of the different profiles is not very intuitive. The following observations can be made of the directivity.

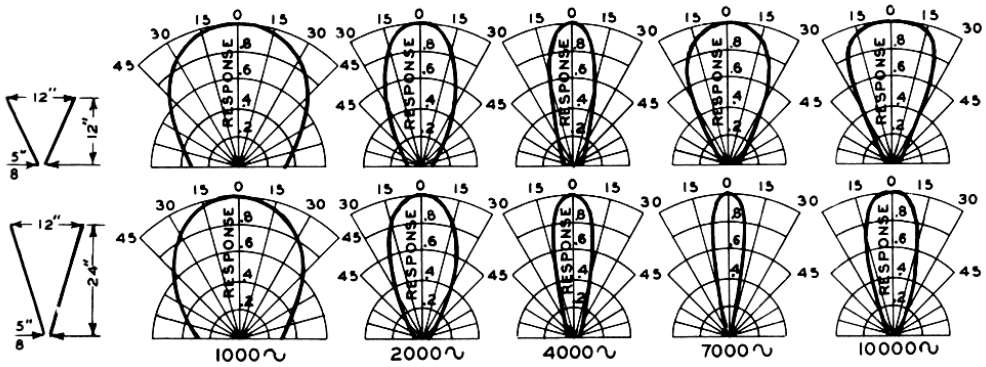

Figure 7.3. Directivity of a conical horn with constant mouth size and varying length. Adopted from [15].

The low frequency directivities are equal. It is dependent only on the mouth size. The short horn has a wider beam width at high frequencies than long horn has.

The beam width is narrowest at the mid frequencies. This is also called midrange beaming [15]. The longer horn has a narrower beam in the 4 kHz and 7 kHz diagrams.

It is safe to assume, that the low frequency directivity of a conical horn is defined by its mouth size as it is with exponential horn geometry.

The directivity of a conical horn is a strongly varying function of frequency and therefore it is not suitable for waveguide as such.

7.3 The exponential and conical horn as a waveguide

The beamwidth of an exponential horn and a conical horn strongly vary as a function frequency. Therefore they are not suitable for a loudspeaker with controlled directivity characteristics. Nevertheless some useful conclusion can be made based on the theory presented before.

Low frequency directivity is dependent only on the mouth size. The cutoff limit is ka < 1 i.e. wavelength is longer than circumference of the horn mouth. When the wavelength is shorter than the mouth circumference, the directivity of the horn is dependent on the geometry.

Because of this, an interesting conclusion can be made about minimum waveguide size for multi-way systems if controllable directivity is desired. Consider a three-way system, with a direct radiating woofer, a midrange driver in a waveguide and a tweeter in a waveguide.

The midrange waveguide size is dependent on the crossover frequency and the woofer directivity, which is related to its size. If ka < 1 for the woofer at the crossover frequency, the midrange waveguide diameter has to be equal to the woofer diameter. Then the directivities will match, according to the theory presented above. If ka > 1 for the woofer at the crossover frequency, the midrange waveguide circumference has to be equal to or larger than the wavelength. Then the directivity of the midrange can be adjusted by the waveguide geometry.

The tweeter waveguide directivity has to match the midrange waveguide directivity at the crossover frequency. With practical crossover frequencies, ka < 1 for the midrange waveguide. Therefore the tweeter waveguide circumference should be equal or larger than the wavelength at the crossover frequency.

Neither exponential nor conical horn shapes are suitable for a constant directivity waveguide as such. The exponential horn beam width decreases towards high frequencies and the beam at high frequencies is too narrow for most applications. The conical horn beam width is narrow at mid frequencies, which is also referred to as midrange beaming. Still these two profiles are a good starting point for horn design and understanding the influence of horn geometry. There are also analytical solutions available for other shapes of horns, but they are even less fit for achieving constant directivity.

8 Using the FEM for modelling waveguides

8.1 Waveguide geometry

The simulation method and measurement were tested with a physical waveguide. The shape of the waveguide was chosen to be simple. The reasoning for this is that the geometry would be easy to manufacture and there would be no measurable geometric error between the modelled and physical prototypes. The properties of the waveguide were chosen to be such that it would have clear directivity characteristics, but its performance would be far from optimal. In other words, the waveguide shape was chosen to be such that it has problems to look for and to solve.

The sound source consists of two parts, which are the waveguide and the tweeter (Figure 8.1, right). The waveguide is a conical shape with a 33° angle tangential to the axis of symmetry. The tweeter is an aluminium dome tweeter with a 19 mm dome diameter. The surround is made of fabric and the diameter width is approximately 3mm. The tweeter is mounted to a faceplate, whose diameter is 40 mm.

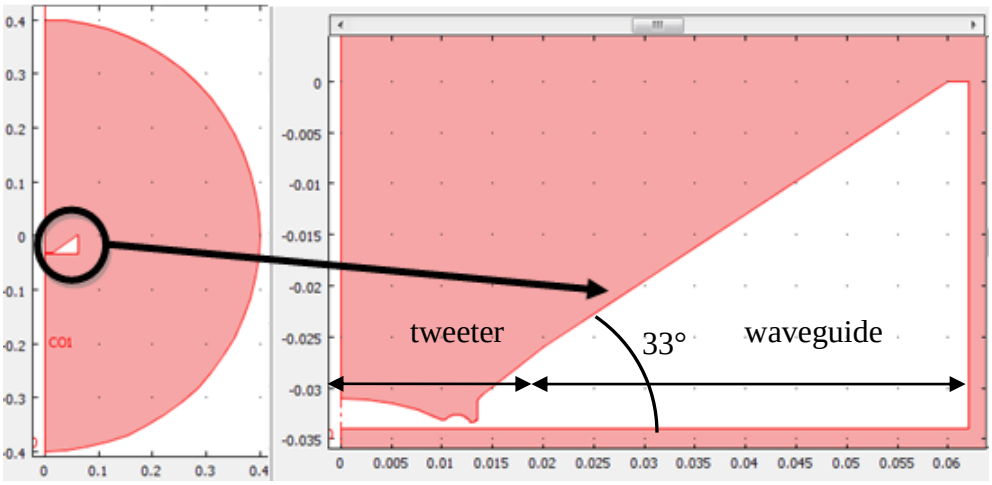

Figure 8.1. Model boundaries (left) and waveguide boundaries (right). Dimensions are in meters.

The waveguide is surrounded with air (Figure 8.1, left). The radius of the air medium is 0.4 meters. The radius of the air space to be modelled is related to the computational cost of the model. The computational cost of solving a model is further discussed in Chapter 3.3.

8.2 Motivation and strategy to simplify geometry

The computational cost of the model is highly dependent on the size and complexity of the geometry. The computational cost of the model can be reduced in the following ways.

Use a 2D axisymmetrical model whenever possible. This is the most significant factor in minimizing model size.

Reduce the area of simulation. For acoustics, this means usually the radius of the modelled air space around the simulated device.

Reduce the details of the geometry. Small details increase the element count of the model. Optimization of the geometry is a matter of knowing what details really affect the result of the simulation. In general, the closer the detail is to the sound source, the greater the effect. Also larger details have a larger effect than small details.

8.3 Modelling the medium and boundary conditions

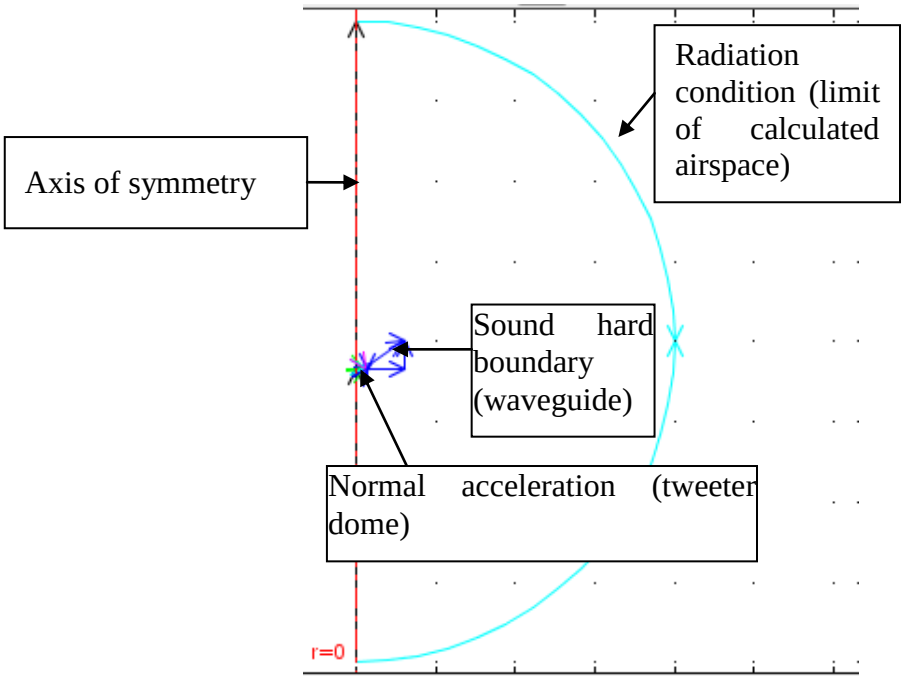

Figure 8.2. The boundaries of an axisymmetric waveguide in 4 sterians airspace.

Boundaries are the geometry edges surrounding the air medium. Boundary condition has to be specified for each boundary.

8.3.1 The medium

The medium is the area or volume in the model where the waves propagate. The properties of the medium have to be correct to achieve accurate results. The medium for acoustical modelling is air. Its density is $\rho = 1.25 kgm^{-3}$ and speed of sound $c = 343 ms^{-1}$, which corresponds to the properties of air at 20 $^{\circ}C$.

8.3.2 Sound hard boundary

The sound hard boundary is a boundary with infinite acoustical impedance. Particle velocity at the boundary is zero. Therefore also particle acceleration is zero at the boundary. The sound hard boundary condition is specified by subtracting the dipole source $\mathbf{q}$ from the gradient of the pressure p and taking the normal vector of the surface with the operator $\mathbf{n}$ [2].

$$\mathbf{n} \cdot \left(\frac{1}{\rho_0} (\nabla p - \mathbf{q}) \right) = 0 \tag{8.1}$$

This boundary condition is used to define all the rigid surfaces of the model

8.3.3 Axisymmetry

This is quite self-explanatory. In other words it is the line which is tangential to the axis of revolution. Of course this boundary needs only to be defined for axisymmetric models.

8.3.4 Normal acceleration

This is the boundary condition that defines the excitation inside the model. The equation for constant acceleration (Equation (8.2) is same as for the sound hard boundary (Equation (8.1) except the acceleration at the boundary is now specified to a_n instead of zero. [2].

$$\mathbf{n} \cdot \left(\frac{1}{\rho_0} (\nabla p - \mathbf{q}) \right) = a_n \tag{8.2}$$

The most straightforward value would be constant acceleration a_n. Constant acceleration equals velocity frequency response, which attenuates 6 dB per raising octave. This is exactly the case with ideal driver movement above its mass-spring resonance frequency. The following assumptions are made with the ideal

acceleration source. First, the diaphragm moves as rigid surface. No breakups of the cone, dome or surround are present. Second, the effect of the voice coil inductance is excluded. Third, electromagnetic field (EMF) from the movement of the voice coil in magnet gap and other dynamic effects are excluded. Fourth, there is no coupling between the acoustical impedance of the air and the diaphragm motion. Pressure at the diaphragm surface does not damp movement of the cone. Therefore the resonances in the acoustic domain tend to be over-exaggerated compared to the reality.

With so many simplifications made, it is fair to question if constant acceleration is realistic enough to model the transducer part of the simulation. However, of the mentioned simplifications, only cone breakups affect the directivity of the system.

On the other hand, it may be a desirable feature to the designer to be able to exclude the nonidealities of the transducer from the contribution of the waveguide.

An external source can be coupled to the model. It is also possible to define a_n as a frequency dependent function.

8.3.5 Radiation boundary condition

Radiation at the boundary can be specified as zero. Therefore there can be no reflections back to the model air domain. This boundary condition is used at the edges of the air domain to represent infinite space outside the modelled space.

8.4 Improving the diaphragm movement model

8.4.1 Motivation for the development of the model

Accuracy of the tweeter radiation used in the FEM model limits the accuracy of the frequency responses of the model. At high frequencies the tweeter radiation starts to dominate the directivity characteristics over the waveguide. Therefore the accuracy of the tweeter model is vital for achieving realistic directivity results at high frequencies. The most difficult part of the tweeter model is to approximate the different radiation characteristics of the several radiating parts. The source of difficulty is that the radiation is dependent on the geometry, location in the geometry and frequency.

This chapter is shows several levels of accuracy improvement for of the tweeter radiation model. First the analogous circuits related to the tweeter and its radiation is introduced. Second, the use of a simple normal acceleration to model the tweeter excitation in the model is discussed. Third, the use of velocity measurements of a known driver as diaphragm excitation is shown. Fourth, is a discussion on how to couple the acoustical and mechanical domain to include the effect of the acoustic pressure on the diaphragm motion.

8.4.2 The equivalent analogous circuit for loudspeaker driver

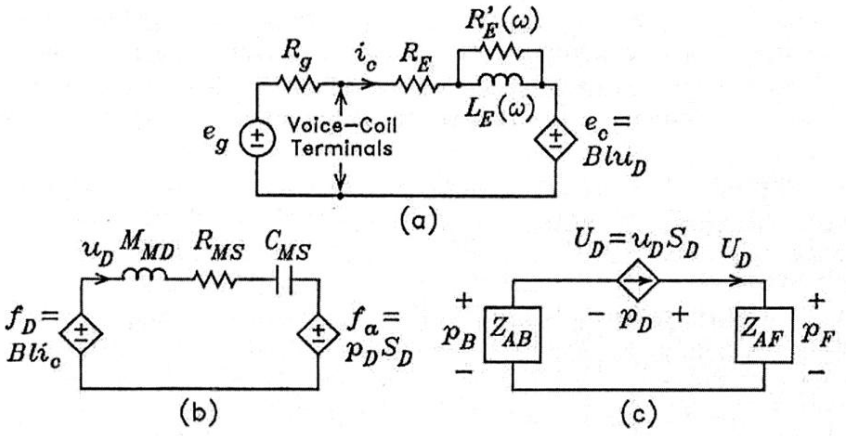

Figure 8.3. Analogous circuit of a transducer. Divided to (a) electrical, (b) mechanical, and (c) acoustical domain. Adopted from [18].

The operation of a transducer can be expressed with an equivalent analogous circuit. There are several ways of presenting the analogous circuit. In the version used, the electrical, mechanical and acoustical domains are separate and then coupled with controlled voltage or current sources (Figure 8.3). The electrical domain consists of the voltage generator e_g and the internal resistance of the generator r_g. The voice coil consists of series resistance of the coil R_e and inductance of the coil L_e shunted with a parallel resistance $R_E^{'}$ to model the damping caused by eddy currents in the iron part of the magnet assembly. Back EMF e_c is modelled by coupling the velocity of the coil u_D from the mechanical domain and multiplying it by the force factor Bl. The mechanical domain consists of the mass of the moving parts M_{MD}, mechanical damping R_{MS} and the compliance of the suspension C_{MS}. The mechanical force f_D from the electrical domain is calculated by multiplication of the electrical current i_c and force factor Bl. The mechanical force f_D from the acoustical domain is

calculated by multiplying the pressure p_D on the diaphragm surface and diaphragm area S_D. The acoustical domain consists on acoustical impedance at front of the diaphragm Z_{AF} and at the back of the diaphragm Z_{AB}. Volume velocity U_D of the diaphragm is coupled from the mechanical domain by multiplying the diaphragm velocity u_D and the area of the diaphragm S_D. The question is, how is the FEM related to all this? This thesis is mostly about modelling the acoustical impedance Z_{AF} at the front of the diaphragm. Because the problem is in a three-dimensional space and also frequency dependent, there is no means to accurately model it using lumped elements. The approach presented crystallizes the idea of modelling the acoustical domain with FEM and how it is connected to the mechanical and electrical domains of the transducer.

8.4.3 Defining location dependent acceleration

The simplest method to excite the FEM model is to specify the diaphragm as constant acceleration boundary condition. The tweeter geometry model (Figure 8.4) has an aluminium dome part, inner half of the suspension, outer half of the suspension, and rigid parts. The simplest approach to specify the dome motion is to specify a constant acceleration for all the moving parts. In that case the modelled directivity becomes quite realistic for wavelengths much longer than the dimensions of the moving parts.

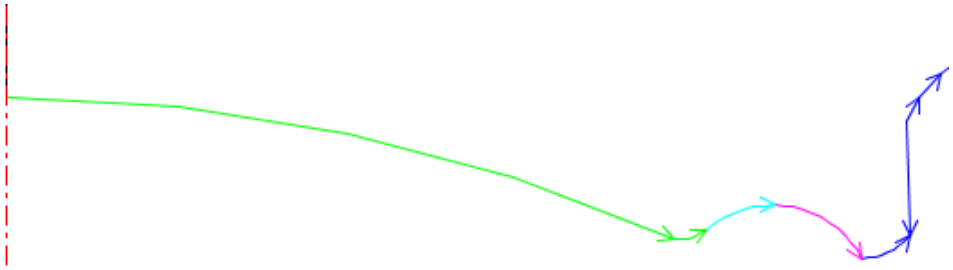

Figure 8.4. The geometry of the tweeter in a model. Aluminium dome (green), inner half of the suspension (cyan), outer half of the suspension (magenta) and rigid parts (blue).

The next improvement is to specify different accelerations for the dome and the surround. Acceleration of the surround has its maximum at the point where it is attached to the dome and the minimum close to the fixing point. For example, the acceleration can be specified to be 0.75 times for the inner part of the suspension and 0.25 for the outer part of the suspensions of the acceleration of the dome.

The root of the problem for defining a realistic diaphragm movement is that the material properties of the dome and surround differ. The aluminium dome moves as a rigid piston in its passband, which is usually about 1 kHz to 20 kHz. The first mechanical eigenmode of the dome is called the dome break-up frequency. Then, the dome no longer moves as a rigid piston. For an aluminium dome this frequency is typically 22 kHz to 30 kHz [19]. However already much below the break-up frequency there is a phase difference between the moving parts of the dome. Usually this phase difference becomes significant about one octave below the break up frequency. For an aluminium dome the range is from 11 kHz to 15 kHz. The sound radiated from the different parts of the dome does not sum up perfectly because of the destructive interference caused by the phase difference. A typical tweeter surround is made of fabric mixed with adhesives. The combination is not very rigid, but the damping properties are excellent. Therefore the surround has resonances in the tweeter frequency range but they are well damped.

8.4.4 Measuring the velocity of the diaphragm

Velocity responses of an aluminium dome and a fabric surround of a tweeter are measured with a laser velocity meter (Figure 8.5). It is clearly seen that the aluminium dome has a higher velocity throughout the frequency range. However, the difference is decreases towards high frequencies. Therefore the radiation caused by the surround starts to dominate at high frequencies. Then the combined radiation approaches the radiation of a ring radiation source, which is much more directive than a piston source. This phenomenon does have an influence on the tweeter high frequency response and directivity. Directivity of the transducer increases toward the high frequencies because of the ring radiator phenomenon.

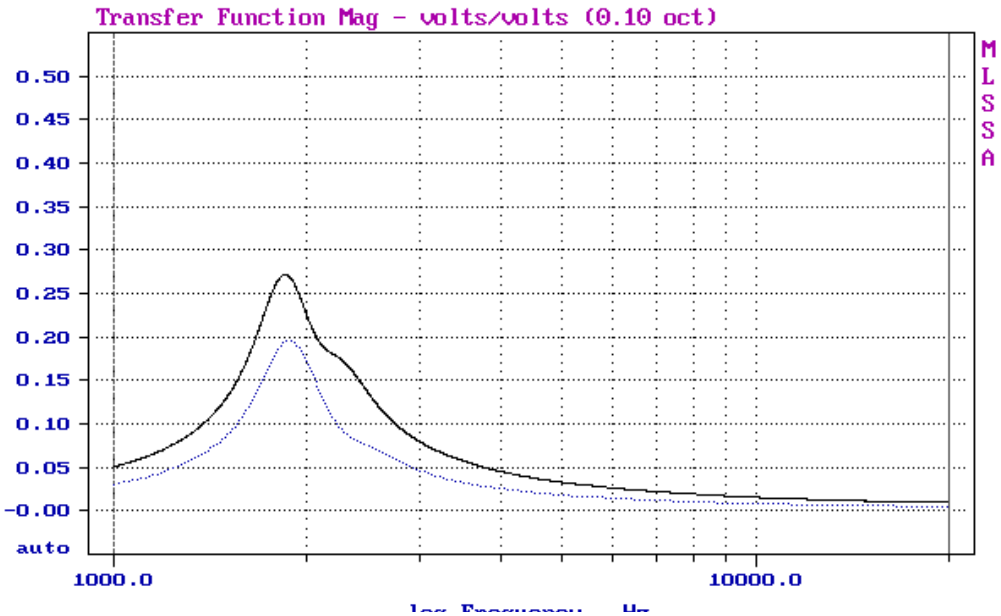

Figure 8.5. Measured velocity [m/s] of dome (black) and surround (blue) of aluminium dome tweeter. One volt excitation.

The velocities of the dome and surround were measured with a laser velocity meter. The transducer was excited with an maximum length sequence (MLS) signal as done in acoustic measurements. The MLS is a pseudo random noise, which consists of a series of impulses. One impulse contains all frequencies and in the frequency domain it is white noise. MLS contains a series of these impulses to improve the energy of the excitation signal and improve signal to noise ratio [20].

The velocity signal of the transducer was sent back to the measurement system, instead of a pressure microphone signal. The boundary condition for the moving part is the acceleration a (Equation (8.3).

$$a = \frac{v}{2\pi f} \tag{8.3}$$

8.4.5 Using measured velocity in the FEM model

The intention was that by combining measurements and simulations a very accurate result could be achieved. Considering again Figure 8.3, now Z_{AF} is simulated with FEM. The transducer velocity u_D is measured. The volume velocity U_D is automatically calculated in the model, because the moving boundary has the information of the diaphragm area. The only missing part in the big picture is the coupling between the air pressure at the diaphragm and mechanical system. The force F_a is the force caused by the acoustic pressure at the diaphragm. It is

calculated (Equation (8.4) by multiplying the pressure at the diaphragm p_D and the area of the diaphragm S_D [18]:

$$F_a = p_D S_D \tag{8.4}$$

Of course the pressure at the diaphragm is not constant, but is location dependent. Fortunately the FEM is able to integrate the complex pressure over the diaphragm surface. The pressure at the diaphragm boundary can be integrated, thereby obtaining the exact force caused by the acoustic pressure. The last step for including diaphragm pressure in the model is to calculate the difference in the acceleration caused by the force caused by the pressure at the diaphragm F_a. If the driver is operating above its mechanical resonance frequency f_s the motion is controlled by the diaphragm mass m. Therefore Newton's second law of motion is valid (Equation (8.5) [21]).

$$F = ma \tag{8.5}$$

The goal is to combine the measured velocity v_D and add the damping caused by the pressure at the dome surface. By combining Equations (8.3), (8.4 and (8.5) an equation can be created which includes the measured acceleration of the moving parts and the damping of the pressure (Equation (8.6). The a_D is the total acceleration at the diaphragm, v_D is the measured velocity of the diaphragm, F_a is the force caused by the acoustic pressure at the diaphragm surface and m_D is the mass of the diaphragm.

$$a_D = \frac{v_D}{2\pi f} - \frac{F_a}{m_D} \tag{8.6}$$

9 Measurement system and visualization

9.1 The selection of the visualization method

Post-processing of the result is significant part of modelling work. First, a meaningful graph should be made so that results can be analyzed and understood. Secondly, the post-processing method should be such that it can be used to visualize physical measurements for comparison.

Various methods for visualizing directivity were introduced in the Chapter 5. For this thesis, the directivity plot was chosen for visualizing the results. The directivity plot is introduced in Chapter 5.8. There are several reasons for selecting the directivity plot as the visualization method.

First, there were no readily available comparison methods for viewing the results from modelling software and physical measurement setups. Writing a post-processing program was inevitable.

Second, the numerical data of the modelled results can be exported with a very good angular resolution. The frequency resolution depends on how many solutions were calculated in the solving process.

Third, the physical model can be measured in the anechoic chamber. The measurement system consists of a turntable and a PC-based measurement program. The measurement program controlled the turntable and excitation signal automatically.

The code for data processing and graph plotting were written in a numerical data processing environment as part of the thesis project (Figure 9.1). Data processing codes had to be individually written for modelling and measurement processing, since the input data formats were different. The code for plotting the results is shared.

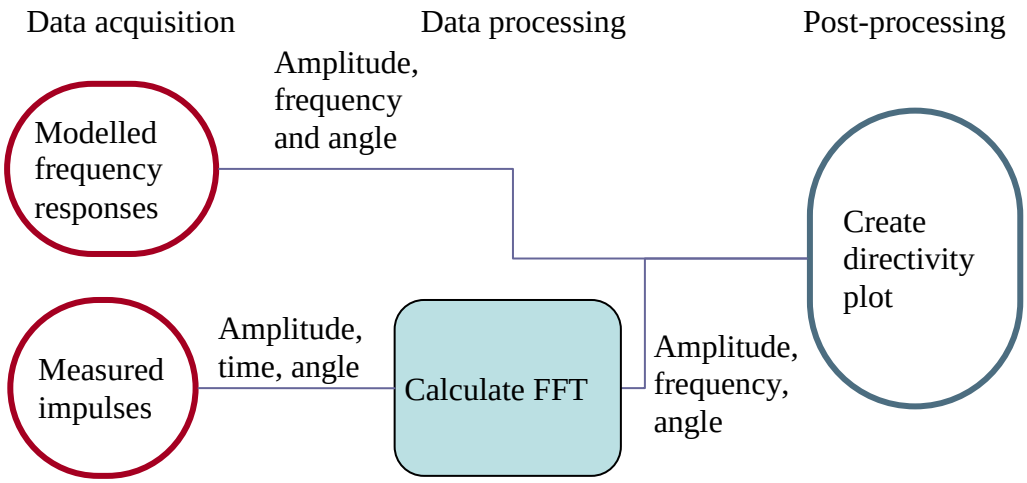

Figure 9.1. The block diagram of data flow to create directivity plots from measured on modelled data.

9.2 Visualizing the directivity of the measurements

The creation of the directivity plot is divided to three parts which are data acquisition, processing the impulses to frequency responses and plotting of the frequency responses (Figure 9.1).

Figure 9.2. Prototype waveguide with a tweeter.

First, the acoustic response of the transducer in the waveguide is measured. The measurements are performed in an anechoic chamber (Figure 9.2). The low frequency limit of the anechoic room is approximately 100 Hz. Loudspeakers are usually omnidirectional at frequencies (below 100 Hz). Therefore the limit is not critical with directivity measurements. In this case the waveguide is used for tweeter (Figure 9.3), whose frequency range is above 1 kHz. Rotation of the waveguide to different angles during the measurement is executed with turn table. The turn table is automatically controlled by the measurement program. Measurements are made at 5° increments from 0° to 180°, which totals 37 measurements. Measurement of one

polar arc is enough, because the waveguide is axisymmetric. Impulse responses of the measurements are stored and named according to the measurement angle.

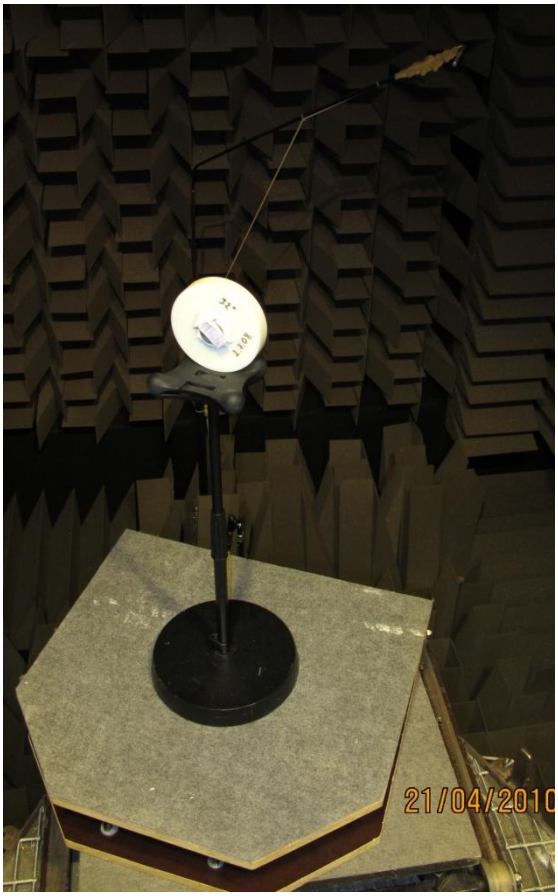

Figure 9.3. The measurement setup of the waveguide. Waveguide is on top of a microphone stand. Stand is on a turning table. Microphone is located in the top right of the figure.

Second, the impulse responses are imported to software to perform a numerical data processing. The frequency responses are calculated with an FFT. All off-axis frequency responses are normalized to the on-axis response. Thus only the directivity can be examined. Also data of the measurement angles, frequency range and title are created.

Third, the directivity plot is created. The inputs are the frequency responses, their respective frequencies and angles. The amplitude contour interval is 3 dB. The directivity is presented from 0° to 90°.

The directivity plot is at its best for examining the directivity of the source. The 3 dB amplitude resolution does limit its usability for amplitude comparison. Therefore it is convenient to exclude the on-axis frequency response information from the graph. This is done by normalizing all frequency responses to the on-axis frequency

response. The result of this normalization is equivalent to the directivity of a source with flat on-axis response.

9.3 Visualizing the directivity of the modelled results

The pressure at the outer boundary of the modelled domain (Figure 8.2) is exported from the modelling software to a numerical format. The exported data contains information of the complex amplitude, frequency and angle.

Directivity data in numerical format is imported to a software to perform numerical analysis. Directivity plot is created with same tool as for measured results (Figure 9.1).

10 Analyzing the simulated waveguide

There are two purposes for this chapter. First is to represent the results found in the directivity plot of the modelled waveguide. Second purpose is to compare the results to known theory of the horns (Chapter 7) and analyze the reasons for the phenomena found in the graphs. The idea is to demonstrate that the modelling tool can be used to understand the reasons behind the phenomena found in the measurement results.

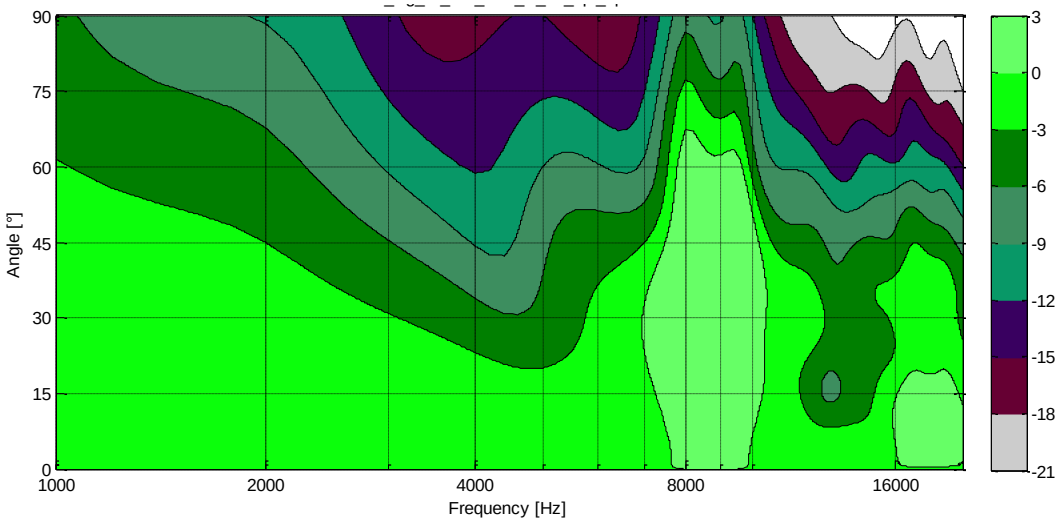

Figure 10.1. Directivity plot of the modelled waveguide.

The directivity plot (Figure 10.1) of the modelled waveguide can be used to analyze the phenomena related to waveguide design. The directivity characteristics of this particular waveguide can be divided to four frequency ranges.

At low frequencies (from 1 to 2 kHz) the waveguide directivity is close to the directivity of a circular piston. The wavelength (from 34 cm – 17 cm) is larger than the circumference of the waveguide mouth. Therefore the directivity of the source is equal to the directivity of circular piston source of the mouth size. This is congruent with the theory of the horn directivity at low frequencies presented in Chapter 7.

At medium frequencies (from 2 to 5 kHz) the beamwidth decreases towards high frequencies. The wavelength (from 17 cm to 7 cm) is shorter than the circumference of the waveguide mouth. Now the shape of the waveguide profile is dominating the directivity. Again this is congruent with the horn theory.

At high frequencies (from 5 to 12 kHz) the diffraction dominates the directivity. The conical waveguide used has a sharp edge at the mouth. The sharp edge can be seen as a impedance discontinuity, which causes diffraction. It is known from the theory that

the diffraction can be seen as a new sound source [15]. In the far field, this new source is out of phase with the direct sound at certain frequency. This phenomenon is almost solely an on-axis frequency response problem, because the off-axis responses are fairly unaffected except the 15° response (Figure 11.3). Even then, the directivity problem arises if a flat on-axis response is desired. The wavelength in the diffraction problem frequency range is approximately 7 cm to 3 cm. The distance from the mouth of the waveguide to the tweeter dome is approximately 2,5 cm. The frequency that correspond a half wavelength of this length is 6800 Hz. As can be seen in the model directivity plot, the diffraction problem is not exactly at one frequency as the theory would suggest. Instead it is smeared to frequency range from 5 kHz to 12 kHz. There are two explanations for this. First explanation is related to the model geometry. The dome is not a point source. Therefore the distance from different parts of the dome to the mouth is not constant. Second explanation is that in theory a plane wave pressure field is assumed. In reality the pressure field is more complex (Figure 10.2) and plane wave approximation is not adequate. The shape of the pressure wave is also frequency dependent.

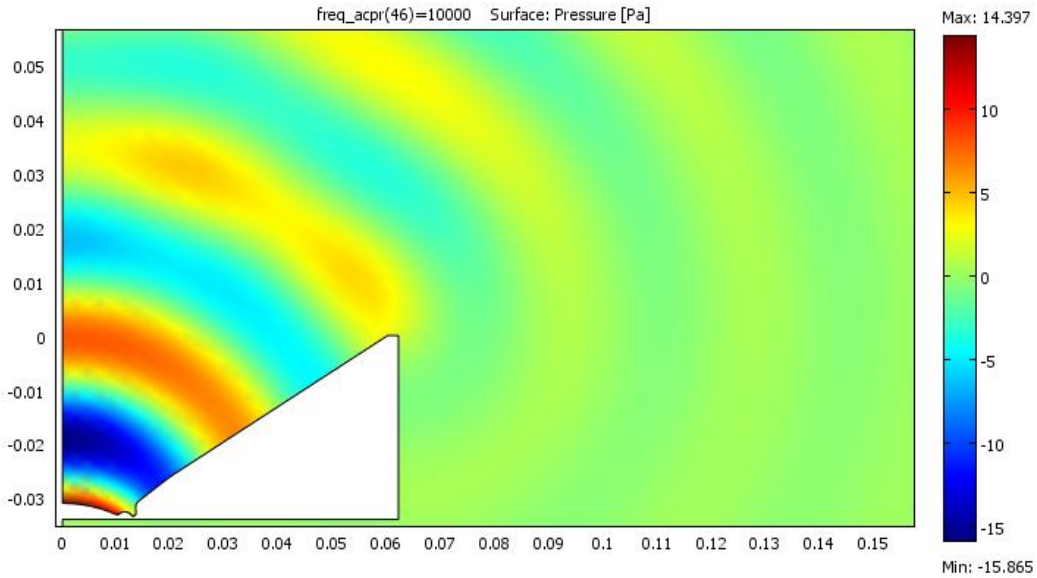

Figure 10.2. Sound pressure around the waveguide at 10 kHz.

The severity of the diffraction problem is emphasized by the axisymmetry (Figure 10.3) because the distance from the tweeter dome to the edge is equal in all azimuth angles. An asymmetrical waveguide would smear the diffraction problem to a broader frequency range.

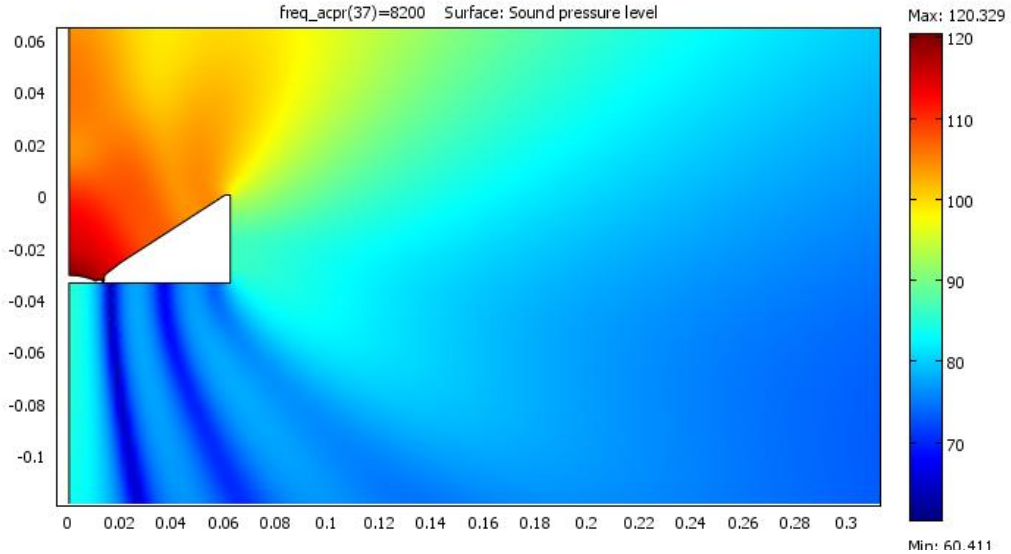

Figure 10.3. Sound pressure level around the waveguide at 8200 Hz.

At very high frequencies (from 12 kHz to 20 kHz) the dome shape starts to affect the directivity, but also the influence of the edge diffraction is present. At 13 kHz, the pressure diffracted at the edge of the waveguide is in phase with the on-axis response. The sum of these sources causes a bump in the on-axis response. Therefore the directivity of the source is increased. Again at 16 – 20 kHz the diffracted wave is out of phase with the direct wave and destructive interference occurs. At high frequencies, the size of the dome circumference is comparable to the wavelength. Therefore the dome geometry affects the directivity. The aluminium dome approximately moves as a rigid piston within the tweeter frequency range. However the surround made of fabric is not rigid at high frequencies.

11 Verifying modelling accuracy

In this chapter are compared the simulated and measured results. First step is to analyze the differences between simulation and measurement and discuss the possible sources of dissimilarities. The second step is to analyze the simulated and measured frequency responses. If the modelled directivity is accurate, then the frequency response should reveal the accuracy of the tweeter driver model used.

11.1 Accuracy of the simulated directivity

The first purpose of this chapter is to present the differences between the measured (Figure 11.1) and simulated directivity (Figure 11.2) of the prototype waveguide. The second purpose is to analyze the difference between these two.

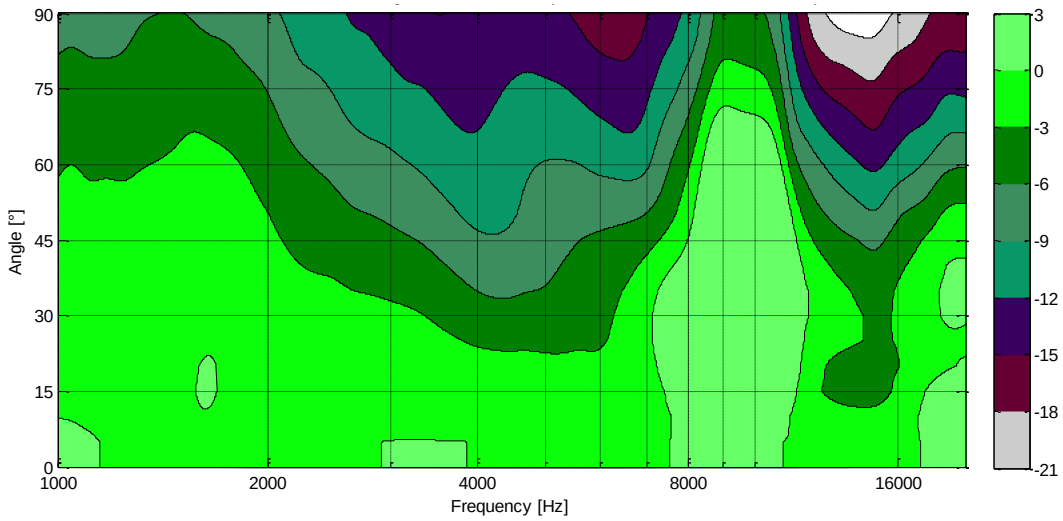

Figure 11.1. Measured directivity plot of the waveguide.

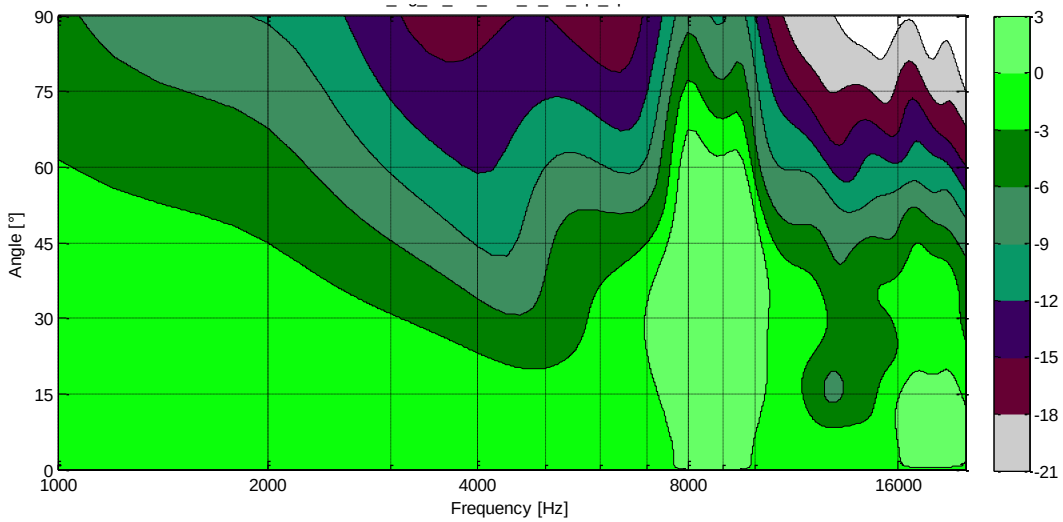

Figure 11.2. Modelled directivity plot of the waveguide.

The first impression is that the measured and modelled directivities are similar. Next the differences are presented in four frequency ranges.

11.1.1 Comparison of the measured and modelled directivity

At low frequencies (from 1 to 2 kHz) the beamwidth of the measured directivity is first increasing and then decreasing. The beamwidth of the modelled results is constantly decreasing.

At mid frequencies (from 2 to 5 kHz) the beamwidth of the measured results is constantly decreasing with little ripple. The -12 dB and -15 dB contours shows decreasing directivity at 5 kHz. Modelled directivity is also decreasing and showing the decrease in directivity at 5 kHz. The distance between equal amplitude contours is smaller in the measurement – in other words the directivity of the source is increasing more rapidly when moving towards the off-axis direction.

At high frequencies (from 5 to 12 kHz) the beamwidth of the measured directivity is rapidly increasing. The centre of the bump is at 10 kHz. The modelled directivity show similar phenomena. The increased beamwidth consist of two merging peaks. Peaks are at 8 kHz and 9.5 kHz.

At very high frequencies (from 12 to 20 kHz) the measured directivity is first increasing and then decreasing. The modelled directivity shows the same phenomena but with more ripple.

11.1.2 Analyzing the differences

At low frequencies (from 1 to 2 kHz) the measured directivity has more ripple. This is probably caused by the measurement jig used under the waveguide (which shown in Figure 9.3).

At mid frequencies (from 2 to 5 kHz) the space between equal amplitude contours is narrower in the modelled directivity. The only reasonable explanation is the 40 cm distance used in model. Thus the far field approximation of the analysis is not valid.

At high frequencies (from 5 to 12 kHz) the width of the bump is very similar, although the exact amplitude contours have differences. The difference between the amplitude contours is largest at large angles. The diffraction causes a resonance

between the low acoustical impedance at the edge of the waveguide mouth and the high acoustical impedance at the throat of the waveguide. There are no losses included in the model but the outer boundary of the modelled air space. Therefore resonant phenomena tend to be exaggerated in the simulation.

At very high frequencies (from 12 to 20 kHz) the dome shape and edge diffraction are combined. Increasing directivity caused by in-phase diffraction can be seen at 13 kHz both in the simulation and the measurement. Also the shapes of decreasing directivity above 16 kHz are similar. The error between the model and the measurement should be highest at high frequencies (e.g. short wavelengths), because the limited detail in the model geometry and finite element size are comparable to the wavelength.

11.2 Accuracy of the simulated frequency response

Main emphasize was on to model the driver excitation in the model. The selected method to validate the accuracy of the driver model is to compare the frequency response of the model against the reality.

The frequency responses of the modelled (Figure 11.3) and measured (Figure 11.4) prototypes are presented at several angles. Frequency responses are presented with a 2 dB amplitude scale to enable critical evaluation of the results. Often a 10 dB scale is used with frequency responses, which would give the illusion of more congruent results. The directivity of the system was discussed in the previous chapter. Therefore phenomena in the frequency responses are emphasized in this chapter, although the directivity of the system can be also analyzed by comparing the off-axis frequency responses.

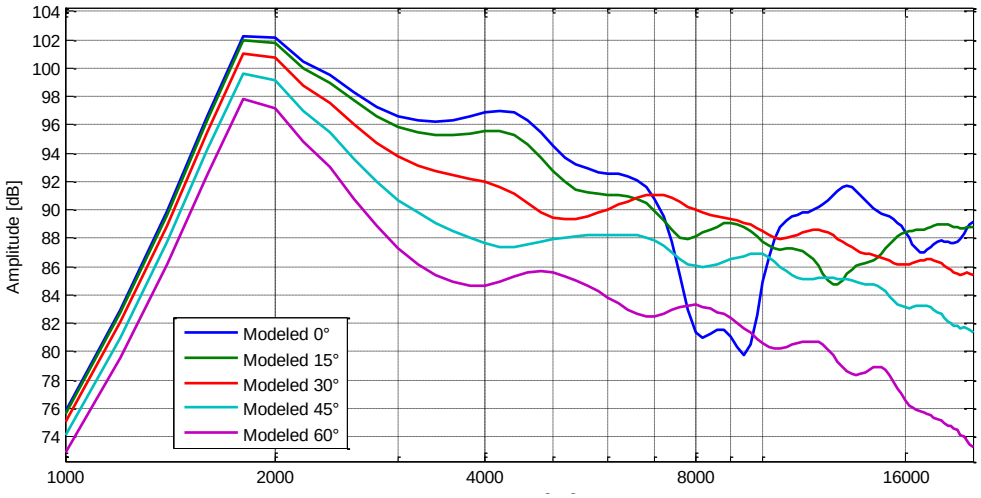

Figure 11.3. The modelled frequency responses of waveguide. From 0° to 60° angles.

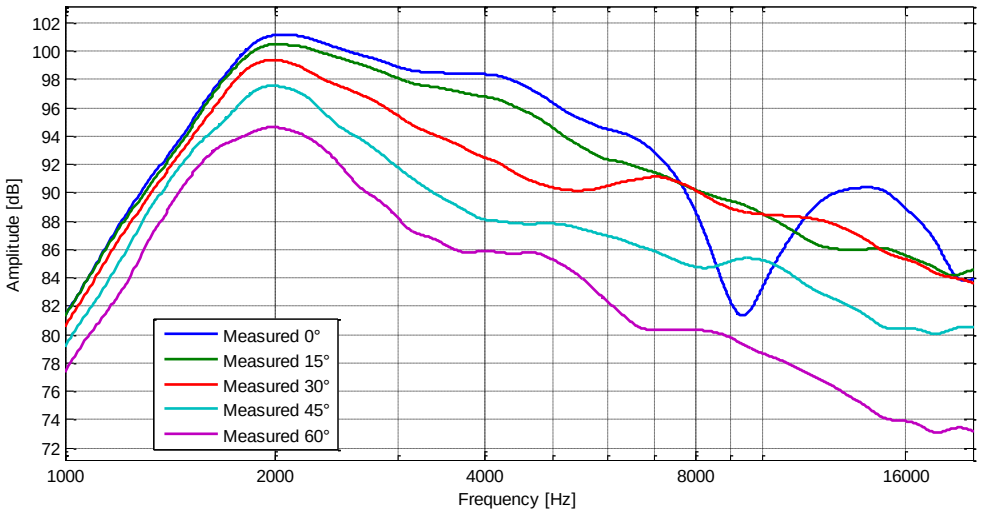

Figure 11.4. The measured frequency responses of the waveguide. From 0° to 60° angles.

11.2.1 Comparing the measured and modelled directivity

Modelled frequency response show a peak of 102 dB at 2 kHz. With measured response the peak is one dB less. The peak is sharper with the modelled result.

Above 3 kHz, the slope of the response is similar in the measured and modelled results. The difference from 3 kHz to 7 kHz is 7 dB both for modelled and measured response. The peak at 4 kHz is present in both graphs, but the peak is 1 dB sharper for the modelled response. The diffraction problem around 9 kHz is also present in the both graphs. For modelled results it consists of two merging notches whereas for the measured response it is one notch. The on-axis response decreases above 12 kHz. The measured result shows more ripple at high frequencies. The modelled angle contours are further apart from each other which equals less directivity.

11.2.2 Analyzing the differences

The peak at 2 kHz of the modelled response is caused by the driver mechanical resonance frequency. In the tweeter model it is expected that the driver is operating above its resonance frequency, which is called the mass controlled region. The acoustical pressure at the dome surface is coupled to the mass of the dome (Equation (8.6)). Therefore the tweeter driver model is not valid close to or below the resonance frequency of the driver. Also the fast decreasing slope of the on-axis response above 2 kHz is also caused by this invalid assumption.

The sharpness of the 4 kHz peak at the modelled result can only be explained by the lack of damping in the resonant phenomena in the model.

The diffraction problem is also resonance related. The possible explanation for the second notch of the modelled result is the lack of internal damping. At very high frequencies (from 12 kHz to 20 kHz) the modelled results show more ripple. Peak of the bump at 12 kHz is 92 dB for both results, but the modelled bump does have a peak in the middle.

12 Conclusions

The purpose of this chapter is to summarize the accuracy and reliability of the FEM method for waveguide modelling. It also outlines the achievements of the work. Lastly the advantages of the tool with engineering problems and the possible future developments are discussed.

12.1 Usability of the simulation

The goal of the thesis is set in the first chapter. The goal is to use, further develop and verify a modelling method for designing waveguide directivity. The finite element method was used to model a conical waveguide. The results were compared to a physical prototype with equal dimensions. The main phenomena of interest were: change of directivity as a function of frequency, diffraction caused by the waveguide mouth edge and the resonant phenomena inside the waveguide.

All the main significant phenomena found in the measured directivity could be found in the modelled directivity, although the accuracy of the frequencies and the amplitudes were varying. Differences between the amplitudes were less than one equal amplitude contour, which means 3 dB accuracy. Model tends to exaggerate the resonant phenomena. This is not necessarily a problem. If the design is optimized in the model to achieve minimum resonance problems, then the real world prototype should be excellent in terms of resonance problems.

The frequency responses of the measured and modelled results show the same phenomena. Differences were less than 2 dB.

Is the model accurate enough to be used in the daily world of engineering problems? It depends on the purpose. For optimizing and visualizing purposes it has shown its value. Often it is enough to be able to visualize the problem by seeing the acoustic field at a certain frequency. Then fast changes to the geometry will show how the phenomenon changes. However prototypes are needed for the final design if the shown accuracy of the model is not enough.

12.2 Guidelines for a successful waveguide design

The design of the prototype waveguide was intentionally far from optimal. Still there is room for conclusions to be made about designing a waveguide with good performance. According to the analysis of the results, the following conclusions can be made for achieving successful waveguide design.

Sharp transitions in geometry should be avoided so as to not excite diffraction. It is shown that smooth a transition to the enclosure baffle is necessary or a severe diffraction problem will occur.

At low frequencies the directivity of the waveguide is comparable to the directivity of a circular piston with a size equal to the mouth of the waveguide. This is consistent with the horn theory.

When the waveguide mouth circumference is comparable to the wavelength, the geometry of the waveguide dominates the directivity. In this frequency range the diffraction problem is worst.

When the circumference of the driver is comparable to the wavelength, the geometry of the driver starts to dominate the directivity characteristics.

An asymmetrical geometry would reduce the diffraction problem by smearing it to a broader frequency range.

12.3 Outputs of the work

There are two unique outputs of the work for which I did not find references in the bibliography. One of them is related to the directivity visualization tool created. It enables an intelligible way to compare the measured and modelled results. One favourable feature is that directivity plots are published by many loudspeaker manufacturers. Therefore there is already plenty of material with which to compare the modelled results without making measurements. The real value of this work is to have a tool for virtually prototyping waveguides. Directivity plots give instant feedback about how the change in the design affected the performance. With compact graphs it is possible to compare the directivity of several prototypes at a glance, whether they are virtual or real.

The second unique output is the improved transducer model. The idea is to combine measurements and modelling. The tweeter output can be also modelled, but as stated before: a modelled result is always second to the real world. The accuracy of the modelled result was improved by combining a laser velocity measurement with the model.

12.4 Advantages of the virtual prototyping

There are several advantages when using FEM modelling. First is the speed of testing the new ideas. It is convenient to try several approaches to find a solution to a problem. Also there is not the problem of storing the tested ideas as with physical prototypes.

The second advantage is the improved visualization of the problem. In a model the full information of the pressure and particle velocity are always known in the modelled area. The information can be processed to achieve the most informative figure of the problem. This improves the insight and intuition related to the acoustical problem. The insight given by the colourful graphs is a great extension to have when intuition is not enough to understand the problem.

The third advantage is related to time and money. With virtual prototypes it is possible to reduce the amount of physical prototypes. This may reduce the cost of the prototypes and also the development time of the product.

12.5 Future work

In general, there seems to be a certain trend for which areas are most suitable for FEM modelling. One common factor is that there is no analytical solution to the problem. The second factor is that prototypes are hard to manufacture or hard to measure. In the field of acoustics, usually the measurement is the troublesome phase. Most problems are 3D. Therefore a huge amount of individual points need to be measured for accurate information of the prototype.

One common problem area is the Helmholtz resonance of a vented enclosure. Current equations for calculating proper port geometry make assumptions that lead to inaccurate results. By using an FEM model the port geometry can be defined right

from the first prototype. It is also possible to use FEM for fluid flow simulation to optimize the port geometry for minimal air turbulence, which causes port noises.

Another possible area of simulation is the enclosure geometry. Diffraction from the enclosure edges is a known problem but few manufacturers pay attention to it.

There is one future improvement for the transducer model presented in Chapter 8.4. The model used in the experiment assumes that the driver is operating above its mechanical resonance frequency. Therefore the movement of the diaphragm is mass controlled. The model does not give correct results if the model is used near the resonance frequency or below it. With a tweeter this is not usually a problem, because the intention is that the resonance frequency of the driver is well below the used frequency range. This assumption is not valid when considering woofers. Therefore a different approach is needed if this method is going to be used for a woofer model. At least two different solutions exist. The first solution would use the impedance response of the woofer to specify the motional impedance. In the second solution, Thiele-Small parameters could be used to replace the simple mass with a damped spring-mass resonator.

13 Bibliography

[1] John Borwick, *Loudspeaker and Headphone Handbook*, 2nd ed.: Focal Press, 1994.

[2] COMSOL, *Acoustics Module User's guide*, 1st ed., 2009.

[3] Frank Ihlenburg, *Finite Element Analysis of Acoustic Scattering*, 1st ed.: Springer, 1998.

[4] O. C. Zienkiewicz and Y. K. Cheung, *The Finite Element Method in Engineering Science*. New York: McGraw-Hill, 1965.

[5] COMSOL, *COMSOL Multiphysics User's guide*, 1st ed., 2009.

[6] Noburo Kyouno, "Acoustic Radiation of a Horn Loudspeaker by the Finite Element Method - Acoustic Characteristics of a Horn Loudspeaker with an Elastic Diaphragm," *J. Audio Eng. Soc.*, vol. 30, no. 12, pp. 896-905, December 1982.

[7] Martin Opitz, "Modern Development Tools for Dynamic Transducers," *AES Convention Paper 5438, Presented at the 111th Convention New York, USA*, September 2001.

[8] Mark Dodd, "The Development of a Forward Radiating Compression Driver by the Application of Acoustic, Magnetic and Thermal Finite Element Methods," *AES Convention Paper 5886, Presented at the 115th Convention New York, USA*, April 2003.

[9] Mark Dodd, "A New Methodology for the Acoustic Design of Compression Driver Phase-Plugs with Concentric Annular Channels," *AES Convention Paper 7258, Presented at the 123th Convention New York, USA*, October 2007.

[10] Dominik Biba, "Modern Development Tools for Dynamic Transducers," *AES Convention Paper 5438, Presented at the 111th Convention Vianna, Austria*, September 2001.

[11] Juha Backman, "Improvement of one-dimensional loudspeaker models," *AES Convention Paper 7253, Presented at the 123rd Convention New York, USA*, October 2007.

[12] Floyd Toole, "Loudspeaker Measurements and Their Relationship to Listener Preferences: Part 1," *J. Audio Eng. Soc.*, vol. 34, no. 4, pp. 227-235, April 1986.

[13] Floyd Toole, "Loudspeaker Measurements and Their Relationship to Listener Preferences: Part 2," *J. Audio Eng. Soc.*, vol. 34, no. 5, pp. 323-348, May 1986.

[14] Floyd Toole, *Sound Reproduction: The Acoustics and Psychoacoustics of Loudspeakers and Rooms*, 1st ed.: Focal Press, 2008.

[15] Harry F. Olson, *Acoustical Engineering*, 1st ed.: D. Van Nostrand Company Inc., 1957.

[16] Leo L Beranek, *Acoustics*, 1st ed.: D. Van Nostrand Company Inc., 1954.

[17] Valtteri Hongisto, *Meluntorjunta*.: Lecture material, Helsinki University of Technology, 2007.

[18] W. Marshall Leach, *Introduction to Electroacoustics and Audio Amplifier Design*, 4th ed.: Kendall Hunt publishing company, 2010.

[19] Martin Colloms, *High Performance Loudspeakers*, 5th ed.: John Wiley & Sons, 1997.

[20] Douglas Rife, "Transfer-Function Measurement Using Maximum-Length

Sequences," *AES Convention Paper 2502, Presented at the 83rd Convention New York, USA*, October 1987.

[21] Isaac Newton, *Mathematical Principles of Natural Philosophy*, 1st ed.: Oxford University, 1729.

[22] Mark Dodd, "The Application of FEM to the Analysis of Loudspeaker Motor Thermal Behaviour," *AES Convention Paper 5521, Presented at the 112th Convention Munich, Germany*, April 2002.

[23] David Smith, "Improvements in Monitor Loudspeaker Systems," *AES Convention Paper 1784, Presented at the 69th Convention Los Angeles, USA*, May 1981.

[24] Earl Geddes, *Audio Transducers*, 1st ed.: Gedlee, 2002.